Targeting resident astrocytes attenuates neuropathic pain after spinal cord injury

Qing Zhao[a, b, 1], Yanjing Zhu[a, 1], Yilong Ren[a, b, 1, §], Lijuan Zhao[a,b], Jingwei Zhao[a, b], Shuai Yin[a, b], Haofei Ni[a, b], Rongrong Zhu*[a], Liming Cheng*[a,b, c] and Ning Xie*[a,b]

[a] Key Laboratory of Spine and Spinal Cord Injury Repair and Regeneration of Ministry of Education, Orthopaedic Department of Tongji Hospital, School of Medicine, School of Life Sciences and Technology, Tongji University, Shanghai, 200065 P. R. China

[b] Division of Spine, Department of Orthopedics, Tongji Hospital, Tongji University School of Medicine, Tongji University, Shanghai, 200065 P. R. China.

[c] Clinical Center for Brain and Spinal Cord Research, Tongji University

* Corresponding author at:

Key Laboratory of Spine and Spinal Cord Injury Repair and Regeneration of Ministry of Education, Division of Spine, Orthopaedic Department of Tongji Hospital, School of Medicine, School of Life Sciences and Technology, Tongji University, 389 Xincun Rd, Shanghai, 200065, P. R. China. Tel: +86 21 66111706. Fax: +86 21 66111329.

E-mail address:

Rong-rong Zhu: rrzhu@tongji.edu.cn,

Li-ming Cheng, limingcheng@tongji.edu.cn,

Ning Xie, nxieprof18@tongji.edu.cn.

[1] These authors contributed equally to this work.

[§] Present address: Department of Orthopedics, Shanghai General Hospital, Shanghai Jiao Tong University School of Medicine, Shanghai 200080, PR China

Running title: Target astrocytes attenuates pain after SCI

Abstract

Astrocytes derive from different lineages and play a critical role in neuropathic pain after spinal cord injury (SCI). Whether selective eliminating these main origins of astrocytes in lumbar enlargement could attenuate SCI-induced neuropathic pain remains unclear. Through transgenic mice injected with an adeno-associated virus vector and diphtheria toxin, astrocytes in lumbar enlargement were lineage traced, targeted and selectively eliminated. Pain-related behaviors were measured with an electronic von Frey apparatus and a cold/hot plate after SCI. RNA sequencing, bioinformatics analysis, molecular experiment and immunohistochemistry were used to explore the potential mechanisms after astrocyte elimination. Lineage tracing revealed that the resident astrocytes but not ependymal cells were the main origins of astrocytes-induced neuropathic pain. SCI induced mice to obtain significant pain symptoms and astrocyte activation in lumbar enlargement. Selective resident astrocytes elimination in lumbar enlargement could attenuate neuropathic pain and activate microglia. Interestingly, the type I interferons (IFNs) signal was significantly activated after astrocytes elimination, and the most activated Gene Ontology terms and pathways were associated with the type I IFNs signal which was mainly activated in microglia and further verified in vitro and in vivo. Furthermore, different concentrations of interferon and Stimulator of interferon genes (STING) agonist could activate the type I IFNs signal in microglia. These results elucidate that selectively eliminating resident astrocytes attenuated neuropathic pain associated with type I IFNs signal activation in microglia. Targeting type I IFNs signal is proven to be an effective strategy for neuropathic pain treatment after SCI.

Keywords

Spinal cord injury, Neuropathic pain, Astrocyte, Origins, Type I interferon.

INTRODUCTION

Spinal cord injury (SCI) can cause sensorimotor deficits and autonomic changes, and approximately 65% of SCI patients suffer chronic, severe neuropathic pain (Henwood and Ellis, 2004). Long-term unrelieved pain will hinder the patient's rehabilitation training, delay functional recovery, and seriously affect the patient's physical and mental health (Henwood and Ellis, 2004; Masri and Keller, 2012). Unfortunately, the effect of current treatments for neuropathic pain is limited (Dworkin et al., 2003). Exploring an effective treatment for neuropathic pain is a major clinical challenge. Astrocytes are the most abundant type of glial cell in the central nervous system (Dozio and Sanchez, 2018). Accumulating studies have shown that astrocytes play a key role in the induction and maintenance of persistent pain (Ji et al., 2019). Cytokines and chemokines produced by astrocytes can powerfully modulate excitatory and inhibitory synaptic transmission in pain circuits, leading to central sensitization, and a transition from acute to chronic neuropathic pain (Ji et al., 2013; Ji *et al.*, 2019; Kawasaki et al., 2008). Inhibiting the proliferation of spinal astrocytes or glial fibrillary acidic protein (GFAP) expression could reduce neuropathic pain (Ji *et al.*, 2019; Tsuda et al., 2011).

Astrocytes are mainly derived from resident astrocytes, NG2 progenitor and ependymal cells (Barnabé-Heider et al., 2010; Ren et al., 2017; Sofroniew, 2009). SCI leads to massive proliferation of resident astrocytes, which are the most abundant and mainly located around the scar (Barnabé-Heider *et al.*, 2010; Sabelstrom et al., 2014). Ependyma is regarded as the main source of endogenous neural stem cells, which widely migrate to injury area and generate the majority of neuroprotective astrocytes after SCI (Barnabé-Heider *et al.*, 2010; Meletis et al., 2008). However, only a small number of ependymal cells could proliferate and migrate to the lesion score after SCI (Ren *et al.*, 2017). NG2 cells, also known as oligodendrocyte progenitor cells, were previously considered to be the component of glial scar after SCI (Church et al., 2016; Hackett and Lee, 2016; Hesp et al., 2015). While, reports about their functions are still controversial, partly because there are

several cell types that up-regulate proteoglycan NG2 after SCI, such as oligodendrocyte progenitor cells, pericytes and macrophages (Huang et al., 2020; Nishiyama et al., 2005). Until now, there is limited data on the main origins of astrocytes-induced neuropathic pain after SCI and whether selectively target these astrocytes could attenuate neuropathic pain is still unclear.

Cervical and thoracic SCI often induce below-level neuropathic pain (Gwak et al., 2012; Shiao and Lee-Kubli, 2018; Vierck, 2020), partly through activating signal transducer and activator of transcription 3 (STAT3)-dependent reactive astrocytes (Ono et al., 2020). The expression of tumor necrosis factor-α (TNF-α), interleukin-1 β (IL-1β) and interleukin-6 (IL-6) in lumbar enlargement was closely associated with below-level neuropathic pain (Honjoh et al., 2019). Mainly because the ascending tracts and superficial dorsal horn (SDH) in lumbar enlargement are closely associated with proprioception and pain signal processing of the lower limbs (Watson, 2012). Thus, targeting the astrocytes in lumbar enlargement may improve neuropathic pain after cervical or thoracic SCI.

A C57BL/6 mouse neuropathic pain model with spinal cord contusion at thoracic level 10 (T10) was constructed. Pain behaviors were measured by an electronic von Frey apparatus and a cold/hot plate. Transgenic mice and lineage tracing were used to determine the main origins of astrocytes-induced neuropathic pain after SCI. To investigate if eliminating these astrocytes in lumbar enlargement could attenuate neuropathic pain after SCI, the transgenic mice, adeno-associated virus (AAV) vector and diphtheria toxin (DT) were used. A previously undescribed improvement effects of targeting these astrocytes on neuropathic pain was identified. Combining with RNA sequencing, bioinformatics analysis, immunohistochemistry, molecular experiment and cultured microglial cells, the potential mechanisms of pain relief were further explored after selective astrocytes elimination.

RESULTS

Resident astrocytes but not ependymal cells were the main origins of astrocytes-induced neuropathic pain after SCI

The construction strategies of transgenic mice were described in **Figure 1A**. The brain slices from C57BL/6-*Foxj1*$^{em1(GFP\text{-}CreERT2\text{-}polyA)Smoc}$ mice showed that choroids plexus in both fourth ventricle and lateral ventricle had been labeled by reporter gene EGFP (**Figure 1B**). However, EGFP positive cells were not found in central canal of spinal cord under normal condition (data not shown), indicating that ependymal cells may not be activated. Therefore, C57BL/6-*Foxj1*$^{em1(GFP\text{-}CreERT2\text{-}polyA)Smoc}$ mice were used to establish contusion SCI models and examine the activation and differentiation of ependymal cells. As reported before (Ren *et al.*, 2017), ependymal cells did not transform to astrocytes in the lesion area (**Figure 1C**). S100 family protein p11 (S100A10) is previously regarded as a marker of neuroprotective astrocytes (Liddelow et al., 2017), but not unique and expressed by various cell types (**Figure 1—figure supplement 1A-C**). Instead, ependymal cells were observed to produce offspring of Tuj1 positive neurons, Oligo2 negative and S100A10 positive cells in epicenter (**Figure 1D-E**). Totally, ependymal cells did not transform to astrocytes as well as Oligo2 positive oligodendrocytes. Therefore, the resident astrocytes but not ependymal cells were the main origins of astrocytes-induced neuropathic pain after SCI.

Using transgenic mice and AAV vectors could selectively target resident astrocytes in lumbar enlargement

The experiment flowchart was described in **Figure 2A**. Compared with the sham group, the SCI group showed increased astrocytes activation (GFAP expression) in ventral spinothalamic tracts (VST, 65.08 ± 2.25 vs. 52.71 ± 1.02), SDH (59.62 ± 2.21 vs. 49.05 ± 1.30, **Figure 2B and Figure 2—figure supplement 1A**), dorsal spinocerebellar tract (DSC, 81.64 ± 3.63 vs. 51.69 ± 1.22), gracile fasciculi (GR, 58.37 ± 1.89 vs. 49.63 ± 0.83) and ventral spinocerebellar tract (VSC, 75.73 ± 2.21 vs.

50.88 ± 1.29). Thus, astrocytes activation in the lumbar enlargement is associated with neuropathic pain after SCI. AAV2/5-GfaABC1D-Cre with a minimal GFAP promoter was used to selectively target resident astrocytes of *Gt(ROSA)26Sor*$^{em1(CAG\text{-}LSL\text{-}tdTomato\text{-}2A\text{-}DTR)Smoc}$ mice. AAV2/5-GfaABC1D-Cre (1:3 dilution, ≥ 0.33E+13 V.G/ml) was injected into the spinal cord of mice (n=3, **Figure 2—figure supplement 1B**). Two weeks after AAV2/5-GfaABC1D-Cre injection, immunofluorescence staining showed that a large number of astrocytes were labelled (**Figure 2—figure supplement 1B**). Meanwhile, almost no tdTomato-positive cells were found in NEUN-positive neurons or Oligo2-positive oligodendrocytes (**Figure 2—figure supplement 1B** and unshown data). To explore the optimal virus concentration, different dilutions including 1:10 (≥1E+12 V.G/ml), 1:100 (≥1E+11 V.G/ml), 1:250 (≥0.4E+11 V.G/ml), 1:500 (≥0.2E+11 V.G/ml), 1:1000 (≥1E+10 V.G/ml) and 1:10000 (≥1E+9 V.G/ml), were set for injection. Immunofluorescence results of spinal cord tissue and slices revealed that the dilution of 1:100 (≥1E+11 V.G/ml) was the optimal intervention concentration for concentrations below 1:100 can hardly target astrocytes (**Figure 2—figure supplement 1B** and unshown data). Then AAV2/5-GfaABC1D-Cre (≥1E+11 V.G/ml) was injected into *Gt(ROSA)26Sor*$^{em1(CAG\text{-}LSL\text{-}tdTomato\text{-}2A\text{-}DTR)Smoc}$ mice 2 weeks before T10 contusion. The labeled resident astrocytes were mainly located in the dorsal side of lumbar enlargement (**Figure 1C**). It was also found that the labeled astrocytes by AAV2/5-GfaABC1D-Cre accounted for 39.03 ± 1.97% astrocytes in dorsal side of SDH (**Figure 1D**). All labeled astrocytes in SCI+AAV+DT group were eliminated after DT injection (**Figure 1C**) and the expression of GFAP was significantly decreased in dorsal side after resident astrocytes elimination (**Figure 1D**).

Selective resident astrocytes elimination in lumbar enlargement attenuated neuropathic pain

Pain-related behaviors were measured with an electronic von Frey apparatus and a cold/hot plate, including mechanical allodynia, thermal and cold hyperalgesia. The pain test was carried out as described in the experiment flowchart (**Figure 2A**). After contusion, the mice showed a complete

hindlimb paralysis and weight loss, and these effects gradually recovered (**Figure 3A-B and Figure 3—figure supplement 1**). The 5 g impactor and 6.25 mm height contusion could induce mice to obtain obvious pain symptoms (**Figure 3C-F**). Mechanical allodynia (reflected by paw withdrawal threshold) occurred at 14 dpi (day post injury, left hindlimb cut-offs vs. baseline; right hindlimb cut-offs vs. baseline), peaked at 28 dpi and sustained until 43 dpi (**Figure 3C-D and Figure 3—figure supplement 2**). Cold hyperalgesia (reflected by paw withdrawal frequency) and thermal hyperalgesia (reflected by paw withdrawal latency) also occurred at 14 dpi, peaked at 43 dpi (**Figure 3E-F and Figure 3—figure supplement 2**). There was no statistical significance in pain-related behaviors, weight and motor function between the sham group and the sham AAV group (**Figure 3A-F and Figure 3—figure supplement 3**).

A total of 36 mice with neuropathic pain were randomly selected to receive diphtheria toxin (DT) injection on 31, 32 and 34 dpi (male= 18, female= 18, SCI+AAV+DT group), and the 36 mice left were classified as control group (male= 18, female= 18, SCI+AAV group). Then pain tests were carried out on 35 dpi after DT injection. Motor function (BMS score) and weight did not change significantly in mice of SCI+AAV+DT group after selective resident astrocytes elimination in the lumbar enlargement (**Figure 3A-B and Figure 3—figure supplement 1**). Mechanical allodynia of the left hindlimb attenuated after selective astrocytes elimination at 35 dpi (first day after astrocytes elimination, **Figure 3C and Figure 3—figure supplement 2**). The pain attenuation effects peaked at 41 dpi (seventh day after astrocytes elimination, **Figure 3C**). The mechanical allodynia of the right hindlimb was relieved after selective astrocytes elimination at 38 dpi (fourth day after astrocytes elimination), and the pain attenuation effects peaked at 41 dpi (**Figure 3D and Figure 3—figure supplement 2**). The attenuation of both cold and thermal pain occurred at 38 dpi, and the pain attenuation effects peaked at 41 dpi (**Figure 3E-F and Figure 3—figure supplement 2**). To further determine the effect of selective astrocytes elimination on hindlimb pain, the pain parameters on left

and right hindlimbs were measured, and observed no obvious difference between them (data not shown). Furthermore, the effect of sex on neuropathic pain, and observed no significant differences between male and female mice (**Figure 3—figure supplement 4-6**). In addition, the effect of DT injection alone on neuropathic pain of wild-type mice was examined after contusion. The contusion models were constructed as mentioned above. The pain response was similar in wild-type mice with or without DT injection (**Figure 3—figure supplement 7**).

Microglia were activated after selective resident astrocytes elimination in lumbar enlargement

Immunofluorescence staining showed that increased activation of astrocytes and microglia and neuron loss were observed in the lesion area in SCI+AAV group and SCI+AAV+DT group after contusion (**Figure 4A, 4C and Figure 4—figure supplement 1**). Compared with SCI+AAV group, enhanced expression of microglia marker Ionized calcium binding adaptor molecule 1 (IBA1) in lumbar enlargement was observed after selective resident astrocytes elimination in SCI+AAV+DT group (**Figure 4B-C**). Furthermore, compared with the SCI+AAV group, the heatmap of RNA-seq analysis results showed that the transcripts of pro-inflammatory microglial marker genes elevated in the SCI+AAV+DT group (**Figure 4D**). As previously reported (Watson, 2012), the three largest ascending tracts, grey matter and SDH were selected to analyze in the immunohistochemistry images. Selective resident astrocytes elimination led to enhanced IBA1 expression in the left DSC, left deep grey matter, left LST, left SDH, left VSC, right GR, right shallow grey matter and right SDH (**Figure 4E-H**). These results indicated that selective resident astrocytes elimination activated the microglia in lumbar enlargement.

Selective resident astrocytes elimination activated the type I IFNs signal in lumbar enlargement

To explore the potential mechanisms of pain attenuation after selective resident astrocytes elimination, RNA-seq and bioinformatics analysis were conducted. RNA-seq analysis revealed that

there were few DEGs between the sham group and sham AAV group (**Figure 5—figure supplement 1A**). Between SCI+AAV group and sham AAV group, 1872 differentially expressed genes (DEGs) were found in SCI+AAV group, including 1654 upregulated and 218 downregulated genes, as shown in volcano map (**Figure 5—figure supplement 1B**). The Gene Ontology (GO) enrichment analysis and KEGG pathway analysis revealed that the abundance of DEGs enriched in several biological processes, which were associated with immune responses including immune system processes, inflammatory responses and innate immune responses (**Figure 5—figure supplement 1C-D**). Compared with SCI+AAV group, the SCI+AAV+DT group (astrocytes elimination group) had 1120 DEGs, including 688 upregulated and 432 downregulated genes. The upregulated DEGs after selective resident astrocytes elimination were mainly enriched in regulating interferons (IFNs) production and signal transduction of type I IFNs (**Figure 5A**) (Borden et al., 2007; Owens et al., 2014; Rothhammer et al., 2016). Protein–protein interaction (PPI) network analysis showed the interaction of these DEGs (**Figure 5B**). Variability was observed between individual animals within the SCI+AAV and SCI+AAV+DT groups, but the expression differences of DEGs in these two groups were significant.

GO enrichment analysis showed that the dominant biological processes were associated with response to virus, immune and type I IFNs responses, including defense response to virus, response to virus, immune system process, cellular response to interferon-alpha/-beta, positive regulation of interferon-alpha/-beta production or secretion, type I interferon signaling pathway, response to interferon-beta, type I interferon biosynthetic process (**Figure 5C**). KEGG pathway analysis found that several signaling pathways were disturbed, including the influenza A, Epstein-Barr virus infection, Herpes simplex virus 1 infection, Measles, Hepatitis C and NOD-like receptor signaling pathways (**Figure 5D**). Heatmap showed significantly elevated transcripts level of critical genes involved in the type I IFNs signaling pathway, including *Jak1/2/3, Ifna16, Cgas, Tyk2, Ifnar1/2,*

Sting1, Irf3/7/9, Ifnb1, and *Ifih1* (**Figure 5E**). Meanwhile, gene set enrichment analysis (GSEA) showed the disturbance of the Janus kinase (Jak)- STAT signaling pathway and cytokine–cytokine receptor interactions (**Figure 5F-G**). Thus, GO enrichment, KEGG pathway, and GSEA analysis results were associated with the type I IFNs signaling pathway (Barrat et al., 2019; Ivashkiv and Donlin, 2014). Totally, these results indicated that selective resident astrocytes elimination activated the type I IFNs signal in lumbar enlargement.

The type I IFNs signal was activated in microglia and associated with pain relief

In order to further verify the results of RNA-seq, RT-PCR was carried out and the results showed the mRNA expression of genes associated with the type I IFNs signaling pathway increased, including *Ifih1(Mad5), Irf3, Irf7, If144, Stat1, Stat2, Parp14, Irf9, Isg15, Oas2, Oas3, Zbp1, Ifit1, Usp18, Dhx58,* and *Eifzak2* (**Figure 6A**). The mRNA expression of type I IFNs signaling genes was similar in wild-type mice with or without DT injection (**Figure 6B**). Furthermore, three critical proteins involved in the type I IFNs signal with significantly increased expression at the transcriptional level were selected, including IRF7, ISG15 and STAT1. Immunofluorescence analysis found that the expression of IRF7, ISG15 and STAT1 proteins was also significantly increased after selective astrocytes elimination (**Figure 6C-D**).

Although various cells in the central nervous system can synthesize and secrete interferons, microglia are resident immune cells and are believed to be the main source of IFN-β within the central nervous system during inflammatory conditions (Owens *et al.*, 2014). Reinert and colleagues (Reinert et al., 2016) identified microglia as the primary producers of type I IFNs. ISG15 and IRF7 were co-located with the microglial marker IBA1 (**Figure 6E**). Thus, ISG15 and IRF7 were mainly expressed by microglia. To further confirmed the expression of type I IFNs signaling factors were derived from microglia, the cultured and lipopolysaccharides (LPS)-activated microglia were used.

Compared with the results for the control microglia (without LPS stimulation), the RT-PCR results revealed that 0.2 μg/mL LPS mainly activated pro-inflammatory microglia, including the pro-inflammatory microglial markers TNF-α, IL-1β, IL-6, and iNOS (**Figure 6G**). Anti-inflammatory microglial markers, including IL-4, TGF-β, IL-10, and Arg-1, were not significantly increased (**Figure 6G**). Additionally, RT-PCR results showed the upregulated mRNA expression of type I IFNs signaling critical genes in LPS-activated microglia, including *Sting1, Stat2, Stat1, Isg15, Irf9,* and *Irf3* (**Figure 6H**). These results indicated that type I IFNs signal was activated in microglia.

In order to further verify the activation of type I IFNs signal in microglia, different concentrations of interferon agonist (Ploy:IC)(Khorooshi et al., 2015) and STING agonist (ADU-S100 and DMXAA) (Li et al., 2023) were used to stimulate microglia at 12 and 24 hours. The mRNA expression of *Ifnb, Isg15, Stat2,* and *Stat1* increased significantly after Ploy:IC stimulation (**Figure 7A-B**). The mRNA expression levels of *Irf7, Ifnb, Stat2, Isg15, Stat1,* and *Irf9* significantly increased after stimulation with ADU-S100 and DMXAA (**Figure 7C-D**). A previous study identified that type I IFNs signals can significantly reduce sensory neuron activation and pain level (Donnelly et al., 2021). Thus, the pain relief after selective resident astrocytes elimination may be associated with the activation of type I IFNs signal in microglia after SCI.

DISCUSSION

Astrogliosis is induced early in neuropathic pain models and sustained for exceptionally long durations, which covers both the acute-to-chronic pain transition and the maintenance phase of pain (Ji *et al.*, 2019). Cytokines and chemokines produced by astrocytes can powerfully modulate excitatory and inhibitory synaptic transmission in pain circuits, leading to central sensitization, and a transition from acute to chronic neuropathic pain (Ji *et al.*, 2013; Ji *et al.*, 2019; Kawasaki *et al.*, 2008). Recently, Kohro et al. (Kohro et al., 2020) identified an SDH-localized Hes5+ astrocytes

population that gated descending noradrenergic control of mechanosensory behaviour via α1A adrenergic receptors (α1A-Ars). Inhibition of locus coeruleus noradrenergic signal transduction to Hes5 + astrocytes could effectively prevent mechanical hyperalgesia induced by capsaicin (Kohro *et al.*, 2020). Astrocytes activation increased in the lumbar enlargement of mice with SCI-induced pain, including the three largest ascending tracts and the SDH. These findings further highlight the importance of astrocytes in processing pain signals and targeting astrocytes may improve neuropathic pain after SCI.

Resident astrocytes maintain stable under normal physiological state and rarely proliferates. SCI leads to massive proliferation of resident astrocytes especially in lesion area and re-express the neural progenitor cell markers, which are the most abundant and mainly located around the scar forming a region complementary to cells derived from ependymal cells (Barnabé-Heider *et al.*, 2010; Sabelstrom *et al.*, 2014). Ependyma is regarded as the main source of endogenous neural stem cells, which widely migrate to injury area and generate the majority of neuroprotective astrocytes after SCI (Barnabé-Heider *et al.*, 2010; Meletis *et al.*, 2008). However, only a small number of ependymal cells could proliferate and migrate to the lesion score after SCI (Ren *et al.*, 2017). Transgenic mice and lineage tracing found that ependymal cells did not produce a large number of astrocytes. Instead, ependymal cells differentiated to Tuj1 positive neurons in epicenter. NG2 cells were previously considered to be the component of glial scar after SCI (Church *et al.*, 2016; Hackett and Lee, 2016; Hesp *et al.*, 2015). However, reports about their functions are still controversial, partly because there are many cell types that up regulate proteoglycan NG2 in the scar and lesion core after SCI (Nishiyama *et al.*, 2005). Totally, through lineage tracing, these findings determined that the resident astrocytes but not ependymal cells were the main origins of astrocytes-induced neuropathic pain after SCI.

One of the novel findings was that selective resident astrocytes elimination in the lumbar

enlargement could attenuate neuropathic pain after SCI. Previously, there were limited data on the association between local astrocytes depletion and neuropathic pain attenuation. Astrocytes were targeted astrocytes in the spinal cord by using GFAP-Cre; *Gt(ROSA)26Sor*$^{em1(CAG\text{-}LSL\text{-}tdTomato\text{-}2A\text{-}DTR)Smoc}$ mice, but the mice were not suitable for labelling astrocytes (**Figure 2—figure supplement 2**). The most reliable mouse strain for targeting astrocytes in vivo is Aldh1l1-Cre/ERT2 mice (Srinivasan et al., 2016). To selectively and locally target astrocytes in spinal cord, instead, selective astrocytes elimination in lumbar enlargement was performed by AAV2/5-GfaABC1D-Cre mediated local astrocytes transduction and DT injection. Several previous studies have reported astrocytes elimination in animal experiments. Through transgenical method, a previous study found that domain-specific depletion of astrocytes in dorsal spinal cord showed atrophy, reduction in the total number of astrocytes, loss of neuropil, and congested neurons (Tsai et al., 2012). However, they did not observe increased inflammation, gliosis, or blood brain barrier (BBB) permeability in these mice (Tsai *et al.*, 2012). They speculated that remaining astrocytes were sufficient for structural maintenance (Tsai *et al.*, 2012). In contrast, domain-specific depletion of astrocytes in ventral spinal cord resulted in abnormal motor neuron synaptogenesis, which was not rescued by immigration of astrocytes from adjoining regions (Tsai *et al.*, 2012). With transgenically targeted DTR and AAV2/5-GfaABC1D-Cre injection, one another study found that DT-mediated ablation of chronic astrocytic scar could significantly prevent axon regrowth after severe SCI of mice (Anderson et al., 2016). Two other studies also found that astrocytes elimination of the whole body impaired redox homeostasis and triggered neuronal loss in the central nervous system, accompanied by myelin sheath loss and motor function impairment (Allnoch et al., 2019; Schreiner et al., 2015). Meanwhile, local astrocytes depletion through local DT injection did not affect astrocytes in other sites as shown in their supplemental information (Schreiner *et al.*, 2015). These results also showed that selective resident astrocytes elimination in the lumbar enlargement does not have a significant impact on

weight and motor function.

The transcripts of pro-inflammatory microglial marker genes elevated and microglia could activate after selective resident astrocytes elimination. As the resident macrophages in the spinal cord, microglia play critical roles in the progress of neuropathic pain (Chen et al., 2018; Salter and Stevens, 2017). However, the role of microglia in chronic inflammatory pain is still controversial (Chen *et al*., 2018). A previous study reported that P2x4 knockout mice exhibit unaltered inflammatory pain (Tsuda et al., 2009). In contrast, Cx3cr1 knockout mice exhibit reduced inflammatory pain (Staniland et al., 2010). Recently, Tansley S *et al.* (Tansley et al., 2022) found that after peripheral nerve injury, microglia will degrade the extracellular matrix structure (neuronal peripheral network, PNN) in lamina I of the spinal dorsal horn, enhance the activity of projection neurons, and induce pain related behaviors. By comparison, Kohno *et al.* (Kohno et al., 2022) described a spinal cord–resident pool of $CD11c^{+}$ microglia that emerges during pain maintenance and contributes to the resolution of neuropathic pain in mice. Interesting, previous evidence indicated that direct activation of astrocytes using an optogenetic approach induces microglial reactivity and pain hypersensitivity (Nam et al., 2016). Thus, microglia act as diverse roles in a pain development and resolution (Sideris-Lampretsas and Malcangio, 2022). Sex differences in the involvement of microglia in mediating chronic pain have been demonstrated (Sorge et al., 2015; Taves et al., 2016). The effect of sex on neuropathic pain was also explored, and observed no significant differences between male and female mice. Thus, there were inconsistent association between sexes and neuropathic pain after SCI (Dominguez et al., 2012; Mapplebeck et al., 2016; McFarlane et al., 2020). Furthermore, the onset of cold/thermal hypersensitivity were delayed than mechanical allodynia, which may be related to the different processing of different types of pain signals.

Among the most significant DEGs after selective resident astrocytes elimination were the genes involved in regulating type I IFNs production, and the signal transduction of type I IFNs was

significantly upregulated. Molecular experiment results also found the mRNA expression of genes associated with the type I IFNs signal increased after selective astrocytes elimination. It has been verified that type I IFNs signal can significantly reduce sensory neuron activation and pain level (Donnelly *et al.*, 2021). Mice with type I IFNs signal deficiency were more sensitive to pain stimuli and had more obvious activation of intense sensory neurons (Donnelly *et al.*, 2021). Thus, type I IFNs signal might be involved in the association between selective resident astrocytes elimination and neuropathic pain attenuation. Although interferons could derive from various cells, myeloid-lineage cells, microglia are resident immune cells in the central nervous system and are believed to be the main source of IFN-β within the CNS during inflammatory conditions (Owens *et al.*, 2014). Reinert and colleagues (Reinert *et al.*, 2016) identified microglia as the primary producers of type I IFNs, and the expression of cGAS and Sting1 were enriched in microglia (Chin, 2019). The association between selective astrocytes elimination, type I IFNs signal and microglia activation remains unclear. Considering that the death or ablation of numerous cell types in CNS including oligodendrocyte could spark activation of microglia (Gritsch et al., 2014), more studies were needed to explore the effect of microglia activation on the association between astrocytes elimination and neuropathic pain attenuation.

There are also some limitations. Although these results determined that the selective resident elimination could significantly attenuate neuropathic pain, astrocyte elimination is difficult to achieve in clinical practice. Instead, these findings provided a strategy to potentially target and activate type I IFNs signal to improve pain after SCI. Additionally, astrocytes elimination may cause many pathophysiological changes in addition to activating type I IFNs signal, the observed effect may be a side effect of the elimination of astrocytes. For these experiments did not identify whether diphtheria toxin-induced cell apoptosis leads to the activation of the type I IFNs signaling pathway in microglia and is not induced only by astrocyte-specific clearance. These experiments in cell culture induced by

LPS were partly to give a possible mechanist explanation, the optimal methods should be performed in primary microglia obtained from SCI+AAV group or SCI+AAV+DT group and compare to shame operated one. Finally, these results also did not provide the rescue experiment, explore the homeostatic function of astrocytes and the roles of interferon agonist (Ploy:IC) and STING agonist (ADU-S100 and DMXAA).

CONCLUSION

Above all, these findings determined that resident astrocytes but not ependymal cells are the main origins of astrocytes participate in neuropathic pain after SCI. The selective resident elimination in lumbar enlargement could significantly attenuate neuropathic pain, and the mechanisms were partly associated with type I IFNs signal activation in microglia (as the schematic diagram shown in **Figure 7—figure supplement 1**). Therefore, targeted intervention on type I IFNs signal may be an effective strategy for neuropathic pain treatment after SCI.

MATERIALS AND METHODS

***Experimental models (organisms/strains)*:**

The experimental procedures were designed to minimize the number of animals used as well as animal suffering. All animal experiments were carried out in accordance with the U.K. Animals (Scientific Procedures) Act, 1986 and associated guidelines, EU Directive 2010/63/EU for animal experiments, and approved by the Institutional Animal Care and Use Committee (IACUC) of the Tongji University School of Medicine (SYXK2019-0005). All transgenic and non-transgenic mice used were derived from in house breeding colonies maintained on C57/BL6 backgrounds. Mice were housed on a 12/12-h light/dark cycle and had food and water available ad libitum. The room temperature and humidity were appropriate. All behavioral testing was performed between 9:00 am

and 5:00 pm. Transgenic mice were purchased from the Model Organisms Centre, Shanghai and the Jackson Laboratory. To target spinal cord ependymal cells, C57BL/6-*Foxj1*$^{em1(GFP\text{-}CreERT2\text{-}polyA)Smoc}$ mice (Cat# NM-KI-200133, the Model Organisms Centre) were used in this experiment. C57BL/6-*Foxj1*$^{em1(GFP\text{-}CreERT2\text{-}polyA)Smoc}$ mice were under the control of promoters with specific expression in ependymal cells (FoxJ1), which have been widely used for identification of cells that express Foxj1 in the central nervous system and peripheral organs (Barnabé-Heider *et al.*, 2010; Ren *et al.*, 2017). *Gt(ROSA)26Sor*$^{em1(CAG\text{-}LSL\text{-}tdTomato\text{-}2A\text{-}DTR)Smoc}$ mice were obtained from *Gt(ROSA)26Sor*$^{em1(CAG\text{-}LSL\text{-}RSR\text{-}tdTomato\text{-}2A\text{-}DTR)Smoc}$ mice (Cat# NM-KI-190086, the Model Organisms Centre) crossed with C57BL/6J$^{Smoc\text{-}Tg(CAG\text{-}Dre)Smoc}$ (Cat# NM-TG-00026, the Model Organisms Centre). *Gt(ROSA)26Sor*$^{em1(CAG\text{-}LSL\text{-}tdTomato\text{-}2A\text{-}DTR)Smoc}$ mice carried the reporter gene tdTomato and diphtheria toxin receptor (DTR), which can be used for lineage tracing and selective elimination for specific cell population (Buch et al., 2005; Madisen et al., 2010), including astrocytes (Anderson *et al.*, 2016). GFAP-Cre; *Gt(ROSA)26Sor*$^{em1(CAG\text{-}LSL\text{-}tdTomato\text{-}2A\text{-}DTR)Smoc}$ mice were obtained from *Gt(ROSA)26Sor*$^{em1(CAG\text{-}LSL\text{-}tdTomato\text{-}2A\text{-}DTR)Smoc}$ mice crossed with FVB-Tg$^{(GFAP\text{-}cre)25Mes/J}$ mice (Cat# JAX004600, the Jackson Laboratory). Wild-type C57BL/6J mice were obtained through reproduction. For genotyping, genomic DNA was isolated from ear biopsy for PCR. Transgenic mice and genotyping primers were listed in **Supplementary File 1a**. B6.Cg-*Gt(ROSA) 26Sor* $^{tm9(CAG\text{-}tdTomato)Hze}$/J mice (Cat# JAX007909, the Jackson Laboratory) were used for the AAV2/5-GfaABC1D-Cre test experiment. A total of 132 *Gt(ROSA)26Sor*$^{em1(CAG\text{-}LSL\text{-}tdTomato\text{-}2A\text{-}DTR)Smoc}$ mice aged 2 months and older were randomly and equally divided into the following groups: the sham group (male=15, female=15), sham AAV group (male=15, female=15), SCI+AAV group (male=18, female=18), and SCI+AAV+DT group (male=18, female=18). Three or more independent experiments were performed.

Spinal cord contusion model and motor function test

Thoracic spinal cord contusion, a widely used SCI model for neuropathic pain (Kramer et al., 2017), and the MASCIS Impactor Model III (W.M. Keck Center for Collaborative Neuroscience, Rutgers, the State University of New Jersey, USA) were applied (Duan et al., 2021). Briefly, mice were weighed and deeply anaesthetized with isoflurane evaporated in a gas mixture containing 70% N_2O and 30% O_2 through a nose mask. The back skin was shaved and cleaned with 75% alcohol. A laminectomy at T10 was performed to remove the part of the vertebra overlying the spinal cord, exposing a circle of dura through an operating microscope (Zeiss, Germany) and rodent stereotaxic apparatus (RWD Life Science Co.,Ltd, Shenzhen, China). The spinal column was stabilized using lateral clamps over the lateral processes at T9 and T11. Contusion was performed at T10 with a 5 g impactor and 6.25 mm height with a force of about 60kdyn, which could cause a moderate injury as previously reported (Wu et al., 2013; Wu et al., 2014), and then the wound was sutured. Mice had received natural illumination to keep warm before and after the surgery. The following symbols were indicators of a successful contusion model: (1) the impact point was located in the middle of T10, (2) paralysis of both hindlimbs occurred after awakening, (3) the cut-offs of mechanical pain were lower than their baselines. Unsuccessful models were excluded in the following experiment and analysis. Sham mice underwent laminectomy but not contusion. Urine was manually expressed from the bladders of the injured mice twice per day until autonomous urination recovered. Hindlimb motor function was tested in an open field chamber on days 0, 1 and 3 after SCI and weekly for up to 6 weeks. The Basso Mouse Scale (BMS) (Basso et al., 2006) was applied to quantify motor function by two investigators blinded to the genotypes and group assignments.

Measurement of mechanical sensitivity with an electronic von Frey apparatus

The mechanical allodynia of the hindlimbs was measured by the electronic von Frey apparatus (IITC Life Sciences, Woodland Hills, CA) as previously reported (Cunha et al., 2004; Martinov et al., 2013), which is a sensitive, objective and quantitative measurement tool for mechanical sensitivity in rodent

models with pain (Cunha *et al.*, 2004; Martinov *et al.*, 2013). The electronic von Frey apparatus has a pressure-meter which consisted of a hand-held force transducer fitted with a 0.5 mm^2 polypropylene tip (Cunha *et al.*, 2004). When positive response appeared, the intensity of the stimulus was automatically recorded. The investigators were proficiency trained in advance to use the polypropylene tip vertically to the central of plantar. Briefly, mice were placed on a wire mesh platform in individual Plexiglas cubicles and allowed to acclimate to the Plexiglas restraint and testing room for 30 minutes. Before testing, the mice were quiet without exploratory behaviors or defecation, and not resting on their paws (Cunha *et al.*, 2004). The average interstimulus interval was 2 minutes. Polypropylene tip was applied a vertical and gradual increase force to the plantar surface of the left and right hindlimbs for 3-4 seconds, or until a positive response appeared. Behaviours that were considered positive responses to the filament included brisk paw withdrawal, flinching, hunching of the back, licking of the stimulated area, and escape responses (Wu et al., 2016). All animals underwent 2 trials (5 measurements/trial) at 24 and 48 hours before contusion to calculate the average plantar paw withdrawal threshold of both hindlimbs at baseline. The measurement of post-contusion withdrawal thresholds was performed in a blinded fashion by two independent investigators at 2, 3, 4, 5, and 6 weeks after contusion. These timepoints were chosen for the nociceptive assays to calculate BMS scores was to avoid the issue of motor impairment for reflex-based assays, and these mice could maintain a standing posture from 2 weeks after contusion on.

Analgesia test for thresholds of cold and thermal pain

Cold and hot plate (Cat# YSL-21; Shanghai Yuyan Instruments Co., Ltd. China) was used to assess cold and thermal pain as previously reported (Carozzi et al., 2013; Wu *et al.*, 2016). Cold and thermal pain tests of the hindlimbs were conducted one day after mechanical allodynia measurement. Before testing, mice were also transferred into the testing room to acclimate to the environment for 30

minutes. The temperatures of 0°C (cold stimulus) and 50°C (hot stimulus) were used to measure the thresholds for noxious heat and cold, respectively (Wu *et al.*, 2016). To avoid tissue injury, temperatures of 0°C (cold stimulus) for 5 minutes and 50°C (hot stimulus) for 30 seconds were set as the cut-off points. The positive response included licking, jumping or hind paw withdrawal. The paw withdrawal latency (for hot stimuli) and paw withdrawal frequency (for cold stimuli) of positive responses were recorded. For hot stimuli, the paw withdrawal latency means the period from touching the hot plate to the emergence of positive response. For cold stimuli, the paw withdrawal frequency means the number of nociceptive responses observed in 5 minutes on cold plate. The tests were carried out 24 hours before contusion and 2, 3, 4, 5, and 6 weeks after contusion. The analgesia test for thresholds of cold and thermal pain were conducted by two investigators blinded to the groups and experimental conditions.

AAV2/5-GfaABC1D-Cre and DT injection

AAV2/5 with the GfaABC1D promoter (AAV2/5-GfaABC1D-Cre) was used to target Cre recombinase expression exclusively in astrocytes (Anderson *et al.*, 2016). The 681 bp GFAP promoter, GfaABC1D, was derived from the 2.2kb human GFAP promoter gfa2. Importantly, the GfaABC1D promoter is about twice as active as gfa2 with smaller size, which is better suited to viral vectors (Lee et al., 2008; Yu et al., 2020). The expression of cargo genes under the GfaABC1D promoter in astrocytes is highly efficient and specific (Yu *et al.*, 2020). Previous study reported that AAV2/5 predominantly labeled astrocytes, displaying robust co-localization of reporter gene (eGFP) with the astrocytic marker, GFAP (Ortinski et al., 2010). The AAV2/5 vector with a minimal GFAP promoter (AAV2/5-GfaABC1D-Cre) has been regarded as the most reliable viral approach and widely used to target astrocytes (Yu *et al.*, 2020). AAV2/5-GfaABC1D-Cre was purchased from Shanghai Taitool Bioscience Co., Ltd. (Cat# S0611-5, ≥1E+13 V.G/ml). AAV2/5-GfaABC1D-Cre was injected into *Gt(ROSA)26Sor*$^{em1(CAG\text{-}LSL\text{--}tdTomato\text{-}2A\text{-}DTR)Smoc}$ mice of SCI+AAV group and

SCI+AAV+DT group 2 weeks before T10 contusion, and into mice of sham AAV group 2 weeks before T10 laminectomy. Sham group mice underwent L4-5 laminectomy but not AAV. Briefly, after precise location of L4-5 spinal cord as previously reported (Rigaud et al., 2008), the back skin was shaved and cleaned with 75% alcohol. A laminectomy was performed at L4-5 as described above. AAV2/5-GfaABC1D-Cre was injected into the both sides of dorsal median of the lumbar enlargement (0.5 mm lateral to midline with a depth of 0.6 mm, 0.4 μL per side, ≥1E+11 V.G/ml in sterile saline), with a Hamilton 33-gauge (33 G) microinjection needle at a speed of 0.2 μL/min. After injection, the needle was held for 5 minutes to avoid liquid reflux. Overall, no obvious tissue injury of spinal cord, no motor and sensory function impairment of hindlimbs were observed during the following two weeks. Spinal cord tissue fluorescence images were taken and handled with a Fluorescence-labeled Organism Bioimaging Instrument (FOBI, Neoscience Ltd., Suwon City, Rep. of Korea) after AAV2/5-GfaABC1D-Cre injection.

Diphtheria toxin (DT) injection

Mice received 500 ng diphtheria toxin (DT, Cat# 150, List Biological Laboratory) in 100 μL distilled, deionized water (ddH_2O) through intraperitoneal injection (i.p.) (Binnewies et al., 2019) on 31, 32 and 34 dpi (days post-injury), when the pain level peaked (the lowest paw withdrawal threshold of mechanical sensitivity). Then, the mice were sacrificed at 1 week after DT injection for RNA sequencing, bioinformatics analysis, immunohistochemistry and molecular experiment.

RNA sequencing (RNA-seq) and bioinformatics analysis

To further evaluate the role of selective astrocytes elimination in gene expression regulation and pain attenuation mechanisms, RNA-seq was used to examine the transcriptomes of lumbar enlargement tissues in sham group (n = 3), sham AAV group (n = 3), SCI+AAV group (n = 3), and SCI+AAV+DT group (n = 3). Previous findings revealed the sex-dependent difference in neuropathic pain after SCI

(Fiore et al., 2022; Stewart et al., 2021). Thus, the lumbar enlargement tissues of female mice were selected for RNA-seq experiment. Briefly, mice were euthanized after terminal anaesthesia by pentobarbital overdose. Spinal cord tissue was dissected from lumbar enlargements (L4-5) at 1 week after selective astrocytes elimination, with a dissecting microscope, and 2 mm segments were harvested and marked. A total of 12 samples were sent to the Beijing Genomics Institute (BGI) Company (Shenzhen, China) in solid carbon dioxide for further RNA-seq analysis, and sequencing was performed on a DNBSEQ platform at BGI Company. Bioinformatics analysis, including Gene Ontology (GO) enrichment, Kyoto Encyclopedia of Genes and Genomes (KEGG) pathway, gene set enrichment analysis (GSEA) and protein–protein interaction (PPI) network analysis, was carried out with the online platform Dr. Tom (BGI Company). Only genes with transcripts per million (TPM) > 1 were analyzed. Differentially expressed genes (DEGs) were identified using the DEGseq method and screened with the criteria of q value ≤ 0.05 and $\log_2 FC \geq 0.6$, where FC represents the fold change. False discovery rate (FDR) method was used to adjust for multiple comparisons to generate q-values in RNA-seq study. The normalized enrichment score (NES) was utilized to select the most activated and inactivated GO terms and pathways. The sequence and sample data have been deposited in the NCBI database under Sequence Read Archive (SRA) with Bioproject identification number PRJNA847704 (Accession number: SRR19611667 - SRR19611678). The single-cell RNA sequencing (scRNA-seq) results were analyzed through online data from injured mouse spinal cords (https://jaeleelab.shinyapps.io/sci_singlecell/) (Milich et al., 2021).

Immunofluorescence staining and analysis

Immunofluorescence staining procedures were conducted as described previously (Ren *et al.*, 2017). After post-fixation and cryoprotection, a dissected 6 mm segment of spinal cord centred around the injury epicentre, or a 2 mm segment of the lumbar enlargement (L4-5), was coronally sectioned at 12 μm thickness and thaw-mounted onto Superfrost Plus slides (Citotest Labware Manufacturing Co.,

Ltd.). The primary antibodies used were as follows: glial fibrillary acidic protein (GFAP, Cat# ab4674, Abcam, 1:500), Neuronal nuclear antigen (NEUN, Cat# ab190565, Abcam, 1:500), Tubulin beta III (Tuj1, Cat# MAB1637, Millipore, 1:500), Ionized calcium binding adaptor molecule 1 (IBA1, Cat# 016-20001, Wako, 1:500), Oligodendrocyte Transcription Factor 2 (Olig2, Cat# AF2418, R&D system, 1:500), S100 Calcium Binding Protein A10 (S100A10, Cat#11250-1-AP, Protein Tech, 1:250), Interferon-stimulated Gene 15 (ISG15, Cat# sc-166755, Santa Cruz, 1:50), Interferon regulatory factor 7 (IRF7, Cat# sc-74471, Santa Cruz, 1:50), Signal transducer and activator of transcription 1 (STAT1, Cat# ab109461, Abcam, 1:150),. The secondary antibodies were Alexa® Fluor 488 (Cat# abs20019A, Absin, 1:500), Alexa® Fluor 488 (Cat# A-32814, Invitrogen, 1:500), Alexa® Fluor 488 (Cat# A-32766, Invitrogen, 1:500), Alexa® Fluor 555 (Cat# A-32773, Invitrogen, 1:500), Alexa® Fluor 594 (Cat# ab150176, Abcam, 1:500), and Alexa® Fluor 647 (Cat# A-32795, Invitrogen, 1:500). The nuclei were stained with 4′,6-diamidino-2-phenylindole (DAPI, Cat# C1002, Beyotime Institute of Biotechnology), and fluorescence images were taken by confocal microscopy (LSM 700, Carl Zeiss, Jena, Germany). Image acquisition was performed with ZEN 2.3 (blue edition, Carl Zeiss), and micrographs were assembled using Adobe Illustrator CC 2018. As previously reported (Watson, 2012), we selected four regions in the lumbar enlargement to analyze in the immunohistochemistry images, including three largest ascending tracts and SDH. The three largest ascending tracts were (1) the gracile and cuneate fasciculi (GR and CU, respectively); (2) the lateral, dorsolateral and ventral spinothalamic tracts (LST, DLST, and VST, respectively); and (3) the dorsal and ventral spinocerebellar tracts (DSC and VSC, respectively). These tracts are closely associated with proprioception and sensation (Watson, 2012). For immunofluorescence analysis of lumbar enlargement, three sections were randomly selected to delineate the three tracts and SDH (3 areas per tract/SDH), then the 160 μm × 160 μm images were exported as single channel images through ZEN 2.3 (blue edition). Lesion area covered the lesion core, rostral and caudal injured spinal cords with a

distance of 500 μm from lesion core, respectively. A total of three sections (8 areas of rostral and 8 of caudal injured spinal cords per section) were randomly selected per mice. Then the 160 μm × 160 μm images were exported by ZEN 2.3 (blue edition). Image-J software with customized macros was used to quantify the fluorescence intensity of proteins including the GFAP, Tuj1, IBA1, ISG15, IRF7 and STAT1 in the images mentioned above. For sham group and treatment groups, three mice per group were tested.

Microglial culture

To observe the production of type I interferon related factors by microglia after activation, lipopolysaccharides (LPS, Cat# Escherichia coli O111:B4, Sigma-Aldrich) was used activated microglia induced Furthermore, different concentrations of interferon agonist (Ploy:IC (Cat# B5551, APExBIO)) (Khorooshi *et al.*, 2015) and Stimulator of interferon genes (STING) agonist (ADU-S100 (Cat# HY-12885B, MCE) and DMXAA (Cat# HY-10964, MCE)) (Li *et al.*, 2023) were used to stimulate microglia for 12 and 24 hours. Mouse microglial SIM-A9 cells were purchased from ATCC (Cat# CRL-3265, ATCC) and cultured according to ATCC recommended growth conditions in DMEM-F12 (Cat# 11330057, Gibco) containing 10% heat-inactivated FBS (Cat# 16140-071, Gibco) and 5% heat-inactivated horse serum (Cat# 26050-088, Gibco) (Correia et al., 2021). LPS at concentrations of 0.2 μg/mL LPS(Jayakumar et al., 2022) was used to stimulate SIM-A9 cells after they reached 60-70% confluency for 24 h. Microglia and culture medium were collected and centrifuged at 12,000 × g for 5 min to remove debris. The expression of pro-inflammatory and anti-inflammatory microglial marker genes were measured by RT-PCR. After the stimulation by Ploy:IC (2.5μg, 12.5μg, 25μg, 50μg, 100μg, 200μg,), ADU-S100 (0.1μg, 1μg, 10μg, 20μg) and DMXAA (1μg, 5μg, 10μg, 20μg) for 12 and 24 hours, the microglia were also obtained for RT-PCR experiment. Control wells were also established, and the data were analyzed and compared with those of the control wells.

Quantitative real-time PCR (RT–PCR)

The total RNA of cells was isolated with RNAiso plus (Cat# 9108, Takara). The concentration and purity of RNA samples were measured using a Nanodrop ND-2000 (Thermo Science, MA, USA) for further experiments. Five hundred nanograms of RNA was converted to complementary DNA (cDNA), which was synthesized with a PrimeScript reverse transcriptase kit (Cat# RR037A, Takara). RT–PCR was performed using a TB Green TM Premix Ex Taq Kit (Cat# RR820A, Takara) on a Light Cycler Real-Time PCR System (480II, Roche). The primer sequences (Shanghai Generay Biotech Co., Ltd.) were designed through PrimerBank (https://pga.mgh.harvard.edu/ primerbank/) and are listed in **Supplementary File 1b-d**. The relative amounts of mRNA were calculated using the ΔΔCt relative quantification method. *Gapdh* served as the control gene, and the mRNA levels of specific genes were normalized to *Gapdh*. Calculations and statistics were performed in Microsoft Excel version 16.36. Graphs were plotted in GraphPad Prism 8 version 8.4.3.

Statistical analysis

All experiments were conducted with three or more duplicates. All continuous data were shown as mean ± SEM. Two-way ANOVA was performed followed by Student Newman–Keuls post hoc test for continuous data. P values < 0.05 were considered statistically significant. Data analyses were conducted using the Statistical Analysis System (SAS), version 9.4 (SAS Institute, Inc, Cary, NC, USA). Plots were generated using GraphPad Prism 8 software (GraphPad Software, San Diego, CA).

Acknowledgments

These experiments were supported by the International Cooperation Project of National Natural Science Foundation of China (Grant No. 81810001048), the National Natural Science Foundation of China (Grant Nos. 81974190, 82271419, 82225027, 81901902 and 81701217), the National Key

R&D Program of China (Grant No. 2020YFC2008703), Shanghai Rising-Star Program (Grant No. 22QA1408200), the Fundamental Research Funds for the Central Universities (22120220555 and 22120230138), Programs in Emergency and Critical Care Medicine, Shanghai Municipal Health Commission (KPB1702), National Key Specialty Program, National Health Commission of China (GJ2301). We thank Gufa Lin, Bei Ma, Zhourui Wu and Xu Xu of our laboratory for help and advice. We also thank Pianpian Fan (Department of Pediatrics, West China second hospital, Sichuan University) for article grammar check and suggestions.

Ethics

Animals (Scientific Procedures) Act, 1986 and associated guidelines, EU Directive 2010/63/EU for animal experiments, and approved by the Institutional Animal Care and Use Committee (IACUC) of the Tongji University School of Medicine (SYXK2019-0005).

Additional files

Supplementary files

Figure 1-figure supplement 1. S100 family protein p11 (S100A10) expressed by various cell types. (A), S100A10 expressed in astrocytes and neuronal like cells of gray matter. GFAP (red, marker of astrocytes), EGFP (green), S100A10 (white). n = 3 biological repeats. Scale bars had been indicated in pictures. (**B-C**), S100A10 expressed by various cell types at different time after SCI. Figures were analyzed and downloaded through online data from injured mouse spinal cords (https://jaeleelab.shinyapps.io/sci_singlecell/).

Figure 2-figure supplement 1. Astrocytes activation in the lumbar enlargement of neuropathic pain mice. The results of AAV2/5-GfaABC1D-Cre targeted astrocytes in lumbar enlargement. (**A**), images of immunofluorescent staining using GFAP (red) as marker of astrocytes. The location of three largest ascending tracts of lumbar enlargements, including (1) CU, GR; (2) LST, DLST, VST; (3) DSC, VSC, along with SDH and gray matter. CU=cuneate fasciculus, GR=gracile

fasciculus, LST=lateral spinothalamic tract, DLST=dorsolateral spinothalamic tract, VST=ventral spinothalamic tract, DSC=dorsal spinocerebellar tract, VSC=ventral spinocerebellar tract, SDH=superficial dorsal horn. Scale bar, 200μm. (**B**), targeting astrocyte in lumbar enlargement with AAV2/5-GfaABC1D-Cre. 1:3 dilution, ≥ 0.33E+13 V.G/ml; 1:100 dilution, ≥1E+11 V.G/ml. Images of immunofluorescent staining using GFAP (green) and NEUN (white) as characteristic markers of neuron and astrocyte. n = 3 biological repeats. Scale bars had been indicated in pictures.

Figure 3—figure supplement 1. Selective astrocyte elimination in lumbar enlargement attenuated neuropathic pain.

Change of weight (**A-B**), BMS scores (**C-D**) in mice after astrocyte elimination. Sham group, n=30; sham+AAV group, n=30; SCI+AAV group, n=36; SCI+AAV+DT group, n=36. Arrow, 500 ng DT injection was performed on 31, 32 and 34 dpi (days post-injury).

Figure 3—figure supplement 2. Selective astrocyte elimination in lumbar enlargement attenuated neuropathic pain.

Change of mechanical allodynia (**A-B**), cold hyperalgesia (**C**) and thermal hyperalgesia (**D**) in mice after astrocyte elimination. SCI+AAV group, n=36; SCI+AAV+DT group, n=36. Arrow, 500 ng DT injection was performed on 31, 32 and 34 dpi (days post-injury). Left, left hindlimbs; right, right hindlimbs. i.p., intraperitoneal injection. Statistical significance was determined by two-way ANOVA followed by Student Newman–Keuls post hoc test. **P < 0.01, ***P < 0.001, SCI+AAV+DT group vs. SCI+AAV group.

Figure 3—figure supplement 3. Selective astrocyte elimination in lumbar enlargement attenuated neuropathic pain.

Change of mechanical allodynia (**A-B**), cold hyperalgesia (**C**) and thermal hyperalgesia (**D**), weight (**E-F**) in mice of sham group and sham+AAV group. Left, left hindlimbs; right, right hindlimbs.

Figure 3-figure supplement 4. No differences in neuropathic pain were observed between male and female mice. (A-H), Change of mechanical allodynia (A-B, E-F), cold hyperalgesia (C, G) and thermal hyperalgesia (D, H) in mice of SCI+AAV group (n=36) and SCI+AAV+DT group (n=36). Arrow, 500 ng DT injection was performed on 31, 32 and 34 dpi (days post-injury). Left, left hindlimbs; right, right hindlimbs. Values are the mean ± SEM. Statistical significance was determined by one-way ANOVA followed by Student Newman–Keuls post hoc test. *P < 0.05.

Figure 3—figure supplement 5. No significant differences in neuropathic pain were observed

between male and female mice.

Change of mechanical allodynia (**A-D**) in mice of SCI+AAV group and SCI+AAV+DT group after astrocyte elimination. SCI+AAV group, n=36; SCI+AAV+DT group, n=36. Left, left hindlimbs; right, right hindlimbs. Statistical significance was determined by one-way ANOVA followed by Student Newman–Keuls post hoc test. *P < 0.05, ***P < 0.001, Female mice vs. male mice.

Figure 3—figure supplement 6. No significant differences in neuropathic pain were observed between male and female mice.

Change of cold hyperalgesia (**A-B**) and thermal hyperalgesia (**C-D**) in mice of SCI+AAV group and SCI+AAV+DT group after astrocyte elimination.

Figure 3-figure supplement 7. Pain symptoms were similar in wild-type mice with or without DT injection. Mechanical allodynia (**A**), cold (**B**) and thermal (**C**) hypersensitivity test results after DT injection in wild-type mice. n = 8 biological repeats. Values are the mean ± SEM. Statistical significance was determined by two-way ANOVA was performed followed by Student Newman–Keuls post hoc test.

Figure 4-figure supplement 1. Full fluorescence images of lesion area. (**A-B**), the full fluorescence images of lesion area. Images of immunofluorescent staining using GFAP (green), Tuj1 (red) and IBA1 (white) as characteristic markers of astrocyte, neuron and microglia, respectively. n = 3 biological repeats. Scale bar, 200μm.

Figure 5-figure supplement 1. RNA-seq analysis results between SCI+AAV group and sham AAV group. (**A-B**), Volcano maps showed the DEGs between groups. (**C-D**), the GO enrichment and KEGG pathway analysis between the SCI+AAV group and sham AAV group. n = 3 biological repeats.

Figure 7—figure supplement 1. The potential schematic diagram of selective resident astrocytes elimination attenuated neuropathic pain after SCI. (**A**), astrocytes in lumbar enlargement were targeted and selectively eliminated through transgenic mice injected with an adeno-associated virus vector (AAV2/5-GfaABC1D-Cre) and diphtheria toxin. Selective astrocyte elimination in lumbar enlargement could attenuate neuropathic pain after SCI, which were associated with type I IFNs signal and microglia activation. (**B**), the production of type I IFNs. Type I IFNs production is mainly

caused by the contact of innate immune cells (mainly macrophages, microglia and astrocyte in CNS) surface or internal receptors (RIG-I receptor Ifih1/Mda5, Cgas, etc.) with virus specific antigenic substances (DNA, RNA), then through intracellular signal molecule transmission (*Sting, Tbk, Ikk*, etc.), and finally activate the transcription factor IRF3/7 to promote the expression of type I IFNs, including IFN-α and IFN-β. (**C**), the signal transduction of type I IFNs. Type I IFNs bind to the same two membrane spanning polypeptide chains type I IFNs receptor 1/2 (IFNAR1/2) (Borden *et al.*, 2007; Owens *et al.*, 2014) and lead to cross phosphorylation and activation of Tyk2/JaK1. Activation of Tyk2 and JAK1 phosphorylate STAT1/2 to form a heterodimer, which then translocate to the nucleus and associate with IRF9 to further form the heterotrimeric transcription factor complex IFN-stimulated gene factor-3 (ISGF3). Finally, ISGF3 translocate to the nucleus and bind to specific IFN-response elements (ISREs) to control the expression of IFNs-stimulated genes (ISGs) (Rothhammer *et al.*, 2016), including *Isg15, Mx1, Oas1, Oas2, Ifit1, Zbp1*.

Supplementary File 1a. Transgenic mice and genotyping primers.

Supplementary File 1b. Primers for type I interferon signal pathway genes.

Supplementary File 1c. Primers for pro- and anti-inflammatory microglial marker genes.

Supplementary File 1d. Primers for Type I IFN signal related genes.

Data availability

The sequence and sample data have been deposited in the NCBI database under Sequence Read Archive (SRA) with Bioproject identification number PRJNA847704 (Accession number: SRR19611667 - SRR19611678). Any information required to utilize and reanalyze the data reported in this paper is available from the corresponding author upon request (nxieprof18@tongji.edu.cn).

REFERENCES

Allnoch, L., Baumgärtner, W., and Hansmann, F. (2019). Impact of Astrocyte Depletion upon Inflammation and Demyelination in a Murine Animal Model of Multiple Sclerosis. Int J Mol Sci *20*. 10.3390/ijms20163922.

Anderson, M.A., Burda, J.E., Ren, Y., Ao, Y., O'Shea, T.M., Kawaguchi, R., Coppola, G., Khakh, B.S., Deming, T.J., and Sofroniew, M.V. (2016). Astrocyte scar formation aids central nervous system axon regeneration. Nature *532*, 195-200. 10.1038/nature17623.

Barnabé-Heider, F., Göritz, C., Sabelström, H., Takebayashi, H., Pfrieger, F.W., Meletis, K., and Frisén, J. (2010). Origin of new glial cells in intact and injured adult spinal cord. Cell Stem Cell *7*, 470-482. 10.1016/j.stem.2010.07.014.

Barrat, F.J., Crow, M.K., and Ivashkiv, L.B. (2019). Interferon target-gene expression and epigenomic signatures in health and disease. Nat Immunol *20*, 1574-1583. 10.1038/s41590-019-0466-2.

Basso, D.M., Fisher, L.C., Anderson, A.J., Jakeman, L.B., McTigue, D.M., and Popovich, P.G. (2006). Basso Mouse Scale for locomotion detects differences in recovery after spinal cord injury in five common mouse strains. J Neurotrauma *23*, 635-659. 10.1089/neu.2006.23.635.

Binnewies, M., Mujal, A.M., Pollack, J.L., Combes, A.J., Hardison, E.A., Barry, K.C., Tsui, J., Ruhland, M.K., Kersten, K., Abushawish, M.A., et al. (2019). Unleashing Type-2 Dendritic Cells to Drive Protective Antitumor CD4(+) T Cell Immunity. Cell *177*, 556-571.e516. 10.1016/j.cell.2019.02.005.

Borden, E.C., Sen, G.C., Uze, G., Silverman, R.H., Ransohoff, R.M., Foster, G.R., and Stark, G.R. (2007). Interferons at age 50: past, current and future impact on biomedicine. Nat Rev Drug Discov *6*, 975-990. 10.1038/nrd2422.

Buch, T., Heppner, F.L., Tertilt, C., Heinen, T.J., Kremer, M., Wunderlich, F.T., Jung, S., and Waisman, A. (2005). A Cre-inducible diphtheria toxin receptor mediates cell lineage ablation after toxin administration. Nat Methods *2*, 419-426. 10.1038/nmeth762.

Carozzi, V.A., Renn, C.L., Bardini, M., Fazio, G., Chiorazzi, A., Meregalli, C., Oggioni, N., Shanks, K., Quartu, M., Serra, M.P., et al. (2013). Bortezomib-induced painful peripheral neuropathy: an electrophysiological, behavioral, morphological and mechanistic study in the mouse. PLoS One *8*, e72995. 10.1371/journal.pone.0072995.

Chen, G., Zhang, Y.Q., Qadri, Y.J., Serhan, C.N., and Ji, R.R. (2018). Microglia in Pain: Detrimental and Protective Roles in Pathogenesis and Resolution of Pain. Neuron *100*, 1292-1311.

10.1016/j.neuron.2018.11.009.

Chin, A.C. (2019). Neuroinflammation and the cGAS-STING pathway. Journal of neurophysiology *121*, 1087-1091. 10.1152/jn.00848.2018.

Church, J.S., Kigerl, K.A., Lerch, J.K., Popovich, P.G., and McTigue, D.M. (2016). TLR4 Deficiency Impairs Oligodendrocyte Formation in the Injured Spinal Cord. The Journal of neuroscience : the official journal of the Society for Neuroscience *36*, 6352-6364. 10.1523/JNEUROSCI.0353-16.2016.

Correia, S.S., Liu, G., Jacobson, S., Bernier, S.G., Tobin, J.V., Schwartzkopf, C.D., Atwater, E., Lonie, E., Rivers, S., Carvalho, A., et al. (2021). The CNS-penetrant soluble guanylate cyclase stimulator CYR119 attenuates markers of inflammation in the central nervous system. J Neuroinflammation *18*, 213. 10.1186/s12974-021-02275-z.

Cunha, T.M., Verri, W.A., Jr., Vivancos, G.G., Moreira, I.F., Reis, S., Parada, C.A., Cunha, F.Q., and Ferreira, S.H. (2004). An electronic pressure-meter nociception paw test for mice. Brazilian journal of medical and biological research = Revista brasileira de pesquisas medicas e biologicas *37*, 401-407. 10.1590/s0100-879x2004000300018.

Dominguez, C.A., Ström, M., Gao, T., Zhang, L., Olsson, T., Wiesenfeld-Hallin, Z., Xu, X.J., and Piehl, F. (2012). Genetic and sex influence on neuropathic pain-like behaviour after spinal cord injury in the rat. European journal of pain (London, England) *16*, 1368-1377. 10.1002/j.1532-2149.2012.00144.x.

Donnelly, C.R., Jiang, C., Andriessen, A.S., Wang, K., Wang, Z., Ding, H., Zhao, J., Luo, X., Lee, M.S., Lei, Y.L., et al. (2021). STING controls nociception via type I interferon signalling in sensory neurons. Nature *591*, 275-280. 10.1038/s41586-020-03151-1.

Dozio, V., and Sanchez, J.C. (2018). Profiling the proteomic inflammatory state of human astrocytes using DIA mass spectrometry. J Neuroinflammation *15*, 331. 10.1186/s12974-018-1371-6.

Duan, H., Pang, Y., Zhao, C., Zhou, T., Sun, C., Hou, M., Ning, G., and Feng, S. (2021). A novel, minimally invasive technique to establish the animal model of spinal cord injury. Ann Transl Med *9*, 881-881. 10.21037/atm-21-2063.

Dworkin, R.H., Backonja, M., Rowbotham, M.C., Allen, R.R., Argoff, C.R., Bennett, G.J., Bushnell, M.C., Farrar, J.T., Galer, B.S., Haythornthwaite, J.A., et al. (2003). Advances in neuropathic pain: diagnosis, mechanisms, and treatment recommendations. Archives of neurology *60*, 1524-1534. 10.1001/archneur.60.11.1524.

Fiore, N.T., Yin, Z., Guneykaya, D., Gauthier, C.D., Hayes, J.P., D'Hary, A., Butovsky, O., and Moalem-Taylor, G. (2022). Sex-specific transcriptome of spinal microglia in neuropathic pain due to

peripheral nerve injury. Glia *70*, 675-696. 10.1002/glia.24133.

Gritsch, S., Lu, J., Thilemann, S., Wortge, S., Mobius, W., Bruttger, J., Karram, K., Ruhwedel, T., Blanfeld, M., Vardeh, D., et al. (2014). Oligodendrocyte ablation triggers central pain independently of innate or adaptive immune responses in mice. Nat Commun *5*, 5472. 10.1038/ncomms6472.

Gwak, Y.S., Kang, J., Unabia, G.C., and Hulsebosch, C.E. (2012). Spatial and temporal activation of spinal glial cells: role of gliopathy in central neuropathic pain following spinal cord injury in rats. Exp Neurol *234*, 362-372. 10.1016/j.expneurol.2011.10.010.

Hackett, A.R., and Lee, J.K. (2016). Understanding the NG2 Glial Scar after Spinal Cord Injury. Front Neurol *7*, 199. 10.3389/fneur.2016.00199.

Henwood, P., and Ellis, J.A. (2004). Chronic neuropathic pain in spinal cord injury: the patient's perspective. Pain Res Manag *9*, 39-45. 10.1155/2004/863062.

Hesp, Z.C., Goldstein, E.Z., Miranda, C.J., Kaspar, B.K., and McTigue, D.M. (2015). Chronic oligodendrogenesis and remyelination after spinal cord injury in mice and rats. The Journal of neuroscience : the official journal of the Society for Neuroscience *35*, 1274-1290. 10.1523/JNEUROSCI.2568-14.2015.

Honjoh, K., Nakajima, H., Hirai, T., Watanabe, S., and Matsumine, A. (2019). Relationship of Inflammatory Cytokines From M1-Type Microglia/Macrophages at the Injured Site and Lumbar Enlargement With Neuropathic Pain After Spinal Cord Injury in the CCL21 Knockout (plt) Mouse. Front Cell Neurosci *13*, 525. 10.3389/fncel.2019.00525.

Huang, W., Bai, X., Meyer, E., and Scheller, A. (2020). Acute brain injuries trigger microglia as an additional source of the proteoglycan NG2. Acta Neuropathol Commun *8*, 146. 10.1186/s40478-020-01016-2.

Ivashkiv, L.B., and Donlin, L.T. (2014). Regulation of type I interferon responses. Nat Rev Immunol *14*, 36-49. 10.1038/nri3581.

Jayakumar, P., Martínez-Moreno, C.G., Lorenson, M.Y., Walker, A.M., and Morales, T. (2022). Prolactin Attenuates Neuroinflammation in LPS-Activated SIM-A9 Microglial Cells by Inhibiting NF-κB Pathways Via ERK1/2. Cell Mol Neurobiol *42*, 2171-2186. 10.1007/s10571-021-01087-2.

Ji, R.R., Berta, T., and Nedergaard, M. (2013). Glia and pain: is chronic pain a gliopathy? Pain *154 Suppl 1*, S10-s28. 10.1016/j.pain.2013.06.022.

Ji, R.R., Donnelly, C.R., and Nedergaard, M. (2019). Astrocytes in chronic pain and itch. Nat Rev Neurosci *20*, 667-685. 10.1038/s41583-019-0218-1.

Kawasaki, Y., Zhang, L., Cheng, J.K., and Ji, R.R. (2008). Cytokine mechanisms of central

sensitization: distinct and overlapping role of interleukin-1beta, interleukin-6, and tumor necrosis factor-alpha in regulating synaptic and neuronal activity in the superficial spinal cord. J Neurosci *28*, 5189-5194. 10.1523/jneurosci.3338-07.2008.

Khorooshi, R., Mørch, M.T., Holm, T.H., Berg, C.T., Dieu, R.T., Dræby, D., Issazadeh-Navikas, S., Weiss, S., Lienenklaus, S., and Owens, T. (2015). Induction of endogenous Type I interferon within the central nervous system plays a protective role in experimental autoimmune encephalomyelitis. Acta Neuropathol *130*, 107-118. 10.1007/s00401-015-1418-z.

Kohno, K., Shirasaka, R., Yoshihara, K., Mikuriya, S., Tanaka, K., Takanami, K., Inoue, K., Sakamoto, H., Ohkawa, Y., Masuda, T., and Tsuda, M. (2022). A spinal microglia population involved in remitting and relapsing neuropathic pain. Science *376*, 86-90. 10.1126/science.abf6805.

Kohro, Y., Matsuda, T., Yoshihara, K., Kohno, K., Koga, K., Katsuragi, R., Oka, T., Tashima, R., Muneta, S., Yamane, T., et al. (2020). Spinal astrocytes in superficial laminae gate brainstem descending control of mechanosensory hypersensitivity. Nature Neuroscience. 10.1038/s41593-020-00713-4.

Kramer, J.L., Minhas, N.K., Jutzeler, C.R., Erskine, E.L., Liu, L.J., and Ramer, M.S. (2017). Neuropathic pain following traumatic spinal cord injury: Models, measurement, and mechanisms. J Neurosci Res *95*, 1295-1306. 10.1002/jnr.23881.

Lee, Y., Messing, A., Su, M., and Brenner, M. (2008). GFAP promoter elements required for region-specific and astrocyte-specific expression. Glia *56*, 481-493. 10.1002/glia.20622.

Li, N., Wang, C., Zhao, Y., Wang, Y., Gao, T., Yu, Y., Wang, G., and Zhang, L. (2023). STING controls opioid-induced itch and chronic itch via spinal tank-binding kinase 1-dependent type I interferon response in mice. J Neuroinflammation *20*, 101. 10.1186/s12974-023-02783-0.

Liddelow, S.A., Guttenplan, K.A., Clarke, L.E., Bennett, F.C., Bohlen, C.J., Schirmer, L., Bennett, M.L., Münch, A.E., Chung, W.-S., Peterson, T.C., et al. (2017). Neurotoxic reactive astrocytes are induced by activated microglia. Nature *541*, 481-487. 10.1038/nature21029.

Madisen, L., Zwingman, T.A., Sunkin, S.M., Oh, S.W., Zariwala, H.A., Gu, H., Ng, L.L., Palmiter, R.D., Hawrylycz, M.J., Jones, A.R., et al. (2010). A robust and high-throughput Cre reporting and characterization system for the whole mouse brain. Nat Neurosci *13*, 133-140. 10.1038/nn.2467.

Mapplebeck, J.C.S., Beggs, S., and Salter, M.W. (2016). Sex differences in pain: a tale of two immune cells. Pain *157 Suppl 1*, S2-s6. 10.1097/j.pain.0000000000000389.

Martinov, T., Mack, M., Sykes, A., and Chatterjea, D. (2013). Measuring changes in tactile sensitivity in the hind paw of mice using an electronic von Frey apparatus. J Vis Exp, e51212. 10.3791/51212.

Masri, R., and Keller, A. (2012). Chronic pain following spinal cord injury. Adv Exp Med Biol *760*, 74-88. 10.1007/978-1-4614-4090-1_5.

McFarlane, K., Otto, T.E., Bailey, W.M., Veldhorst, A.K., Donahue, R.R., Taylor, B.K., and Gensel, J.C. (2020). Effect of Sex on Motor Function, Lesion Size, and Neuropathic Pain after Contusion Spinal Cord Injury in Mice. J Neurotrauma *37*, 1983-1990. 10.1089/neu.2019.6931.

Meletis, K., Barnabe-Heider, F., Carlen, M., Evergren, E., Tomilin, N., Shupliakov, O., and Frisen, J. (2008). Spinal cord injury reveals multilineage differentiation of ependymal cells. PLoS Biol *6*, e182. 10.1371/journal.pbio.0060182.

Milich, L.M., Choi, J.S., Ryan, C., Cerqueira, S.R., Benavides, S., Yahn, S.L., Tsoulfas, P., and Lee, J.K. (2021). Single-cell analysis of the cellular heterogeneity and interactions in the injured mouse spinal cord. Journal of Experimental Medicine *218*. 10.1084/jem.20210040.

Nam, Y., Kim, J.H., Kim, J.H., Jha, M.K., Jung, J.Y., Lee, M.G., Choi, I.S., Jang, I.S., Lim, D.G., Hwang, S.H., et al. (2016). Reversible Induction of Pain Hypersensitivity following Optogenetic Stimulation of Spinal Astrocytes. Cell Rep *17*, 3049-3061. 10.1016/j.celrep.2016.11.043.

Nishiyama, A., Yang, Z., and Butt, A. (2005). Astrocytes and NG2-glia: what's in a name? Journal of anatomy *207*, 687-693. 10.1111/j.1469-7580.2005.00489.x.

Ono, T., Kohro, Y., Kohno, K., Tozaki-Saitoh, H., Nakashima, Y., and Tsuda, M. (2020). Mechanical pain of the lower extremity after compression of the upper spinal cord involves signal transducer and activator of transcription 3-dependent reactive astrocytes and interleukin-6. Brain Behav Immun *89*, 389-399. 10.1016/j.bbi.2020.07.025.

Ortinski, P.I., Dong, J., Mungenast, A., Yue, C., Takano, H., Watson, D.J., Haydon, P.G., and Coulter, D.A. (2010). Selective induction of astrocytic gliosis generates deficits in neuronal inhibition. Nat Neurosci *13*, 584-591. 10.1038/nn.2535.

Owens, T., Khorooshi, R., Wlodarczyk, A., and Asgari, N. (2014). Interferons in the central nervous system: a few instruments play many tunes. Glia *62*, 339-355. 10.1002/glia.22608.

Reinert, L.S., Lopušná, K., Winther, H., Sun, C., Thomsen, M.K., Nandakumar, R., Mogensen, T.H., Meyer, M., Vægter, C., Nyengaard, J.R., et al. (2016). Sensing of HSV-1 by the cGAS-STING pathway in microglia orchestrates antiviral defence in the CNS. Nat Commun *7*, 13348. 10.1038/ncomms13348.

Ren, Y., Ao, Y., O'Shea, T.M., Burda, J.E., Bernstein, A.M., Brumm, A.J., Muthusamy, N., Ghashghaei, H.T., Carmichael, S.T., Cheng, L., and Sofroniew, M.V. (2017). Ependymal cell contribution to scar formation after spinal cord injury is minimal, local and dependent on direct

ependymal injury. Sci Rep *7*, 41122. 10.1038/srep41122.

Rigaud, M., Gemes, G., Barabas, M.E., Chernoff, D.I., Abram, S.E., Stucky, C.L., and Hogan, Q.H. (2008). Species and strain differences in rodent sciatic nerve anatomy: implications for studies of neuropathic pain. Pain *136*, 188-201. 10.1016/j.pain.2008.01.016.

Rothhammer, V., Mascanfroni, I.D., Bunse, L., Takenaka, M.C., Kenison, J.E., Mayo, L., Chao, C.C., Patel, B., Yan, R., Blain, M., et al. (2016). Type I interferons and microbial metabolites of tryptophan modulate astrocyte activity and central nervous system inflammation via the aryl hydrocarbon receptor. Nat Med *22*, 586-597. 10.1038/nm.4106.

Sabelstrom, H., Stenudd, M., and Frisen, J. (2014). Neural stem cells in the adult spinal cord. Exp Neurol *260*, 44-49. 10.1016/j.expneurol.2013.01.026.

Salter, M.W., and Stevens, B. (2017). Microglia emerge as central players in brain disease. Nat Med *23*, 1018-1027. 10.1038/nm.4397.

Schreiner, B., Romanelli, E., Liberski, P., Ingold-Heppner, B., Sobottka-Brillout, B., Hartwig, T., Chandrasekar, V., Johannssen, H., Zeilhofer, Hanns U., Aguzzi, A., et al. (2015). Astrocyte Depletion Impairs Redox Homeostasis and Triggers Neuronal Loss in the Adult CNS. Cell Reports *12*, 1377-1384. https://doi.org/10.1016/j.celrep.2015.07.051.

Shiao, R., and Lee-Kubli, C.A. (2018). Neuropathic Pain After Spinal Cord Injury: Challenges and Research Perspectives. Neurotherapeutics : the journal of the American Society for Experimental NeuroTherapeutics *15*, 635-653. 10.1007/s13311-018-0633-4.

Sideris-Lampretsas, G., and Malcangio, M. (2022). Pain-resolving microglia. *376*, 33-34. doi:10.1126/science.abo5592.

Sofroniew, M.V. (2009). Molecular dissection of reactive astrogliosis and glial scar formation. Trends in neurosciences *32*, 638-647. 10.1016/j.tins.2009.08.002.

Sorge, R.E., Mapplebeck, J.C., Rosen, S., Beggs, S., Taves, S., Alexander, J.K., Martin, L.J., Austin, J.S., Sotocinal, S.G., Chen, D., et al. (2015). Different immune cells mediate mechanical pain hypersensitivity in male and female mice. Nat Neurosci *18*, 1081-1083. 10.1038/nn.4053.

Srinivasan, R., Lu, T.Y., Chai, H., Xu, J., Huang, B.S., Golshani, P., Coppola, G., and Khakh, B.S. (2016). New Transgenic Mouse Lines for Selectively Targeting Astrocytes and Studying Calcium Signals in Astrocyte Processes In Situ and In Vivo. Neuron *92*, 1181-1195. 10.1016/j.neuron.2016.11.030.

Staniland, A.A., Clark, A.K., Wodarski, R., Sasso, O., Maione, F., D'Acquisto, F., and Malcangio, M. (2010). Reduced inflammatory and neuropathic pain and decreased spinal microglial response in

fractalkine receptor (CX3CR1) knockout mice. J Neurochem *114*, 1143-1157. 10.1111/j.1471-4159.2010.06837.x.

Stewart, A.N., Lowe, J.L., Glaser, E.P., Mott, C.A., Shahidehpour, R.K., McFarlane, K.E., Bailey, W.M., Zhang, B., and Gensel, J.C. (2021). Acute inflammatory profiles differ with sex and age after spinal cord injury. J Neuroinflammation *18*, 113. 10.1186/s12974-021-02161-8.

Tansley, S., Gu, N., Guzmán, A.U., Cai, W., Wong, C., Lister, K.C., Muñoz-Pino, E., Yousefpour, N., Roome, R.B., Heal, J., et al. (2022). Microglia-mediated degradation of perineuronal nets promotes pain. Science *377*, 80-86. 10.1126/science.abl6773.

Taves, S., Berta, T., Liu, D.L., Gan, S., Chen, G., Kim, Y.H., Van de Ven, T., Laufer, S., and Ji, R.R. (2016). Spinal inhibition of p38 MAP kinase reduces inflammatory and neuropathic pain in male but not female mice: Sex-dependent microglial signaling in the spinal cord. Brain Behav Immun *55*, 70-81. 10.1016/j.bbi.2015.10.006.

Tsai, H.H., Li, H., Fuentealba, L.C., Molofsky, A.V., Taveira-Marques, R., Zhuang, H., Tenney, A., Murnen, A.T., Fancy, S.P., Merkle, F., et al. (2012). Regional astrocyte allocation regulates CNS synaptogenesis and repair. Science *337*, 358-362. 10.1126/science.1222381.

Tsuda, M., Kohro, Y., Yano, T., Tsujikawa, T., Kitano, J., Tozaki-Saitoh, H., Koyanagi, S., Ohdo, S., Ji, R.R., Salter, M.W., and Inoue, K. (2011). JAK-STAT3 pathway regulates spinal astrocyte proliferation and neuropathic pain maintenance in rats. Brain *134*, 1127-1139. 10.1093/brain/awr025.

Tsuda, M., Kuboyama, K., Inoue, T., Nagata, K., Tozaki-Saitoh, H., and Inoue, K. (2009). Behavioral phenotypes of mice lacking purinergic P2X4 receptors in acute and chronic pain assays. Mol Pain *5*, 28. 10.1186/1744-8069-5-28.

Vierck, C. (2020). Mechanisms of Below-Level Pain Following Spinal Cord Injury (SCI). J Pain *21*, 262-280. 10.1016/j.jpain.2019.08.007.

Watson, C. (2012). The Somatosensory System. In The Mouse Nervous System, pp. 563-570. 10.1016/b978-0-12-369497-3.10021-4.

Wu, J., Renn, C.L., Faden, A.I., and Dorsey, S.G. (2013). TrkB.T1 contributes to neuropathic pain after spinal cord injury through regulation of cell cycle pathways. J Neurosci *33*, 12447-12463. 10.1523/jneurosci.0846-13.2013.

Wu, J., Zhao, Z., Sabirzhanov, B., Stoica, B.A., Kumar, A., Luo, T., Skovira, J., and Faden, A.I. (2014). Spinal cord injury causes brain inflammation associated with cognitive and affective changes: role of cell cycle pathways. J Neurosci *34*, 10989-11006. 10.1523/jneurosci.5110-13.2014.

Wu, J., Zhao, Z., Zhu, X., Renn, C.L., Dorsey, S.G., and Faden, A.I. (2016). Cell cycle inhibition

limits development and maintenance of neuropathic pain following spinal cord injury. Pain *157*, 488-503. 10.1097/j.pain.0000000000000393.

Yu, X., Nagai, J., and Khakh, B.S. (2020). Improved tools to study astrocytes. Nature Reviews Neuroscience *21*, 121-138. 10.1038/s41583-020-0264-8.

Legends

Figure 1. Ependymal cells did not transform to astrocytes in our transgenic mice. (A), construction strategies of transgenic mice. **(B)**, ependymal cells both in fourth ventricle (4V) and lateral ventricle (LV) had been labeled by reporter gene EGFP (green). n = 6 biological repeats. **(C)**, ependymal cells did not produce astrocytes in the lesion area. n = 3 biological repeats. **(D-E)**, ependymal cells were observed to produce offspring of neurons (Tuj1+, red), Oligo2 (white) negative and S100A10 (white in **D** or red in **E**) positive cells in epicenter. n = 3 biological repeats. 4V=fourth ventricle, LV=lateral ventricle, CB= Cerebellum. Scale bars had been indicated in pictures.

Figure 2. Resident astrocytes in lumbar enlargement were selectively targeted and eliminated. (**A**), the experiment flowchart. (**B**), the histogram and statistical results of GFAP fluorescence intensity. The location of three largest ascending tracts of lumbar enlargements, including (1) CU, GR; (2) LST, DLST, VST; (3) DSC, VSC, along with SDH and gray matter. CU=cuneate fasciculus, GR=gracile fasciculus, LST=lateral spinothalamic tract, DLST=dorsolateral spinothalamic tract, VST=ventral spinothalamic tract, DSC=dorsal spinocerebellar tract, VSC=ventral spinocerebellar tract, SDH=superficial dorsal horn. n = 3 biological repeats. Scale bar, 200μm. Values are the mean ± SEM. Statistical significance was determined by two-way ANOVA followed by Student Newman–Keuls post hoc test. **P < 0.01, ***P < 0.001, Sham group vs. SCI Pain positive (+) group. (**C**), AAV2/5-GfaABC1D-Cre targeted astrocytes were mainly in dorsal side and reflected by tdTomato and GFAP double positive cells in SCI+AAV group, no tdTomato and GFAP double positive cells were found in SCI+AAV+DT group. n = 3 biological repeats. Scale bars had been indicated in pictures. **(D)**, the efficiency of astrocytes labeling and elimination in dorsal side of spinal cord. Immunofluorescence analysis results of GFAP after selective astrocyte elimination. Values are the mean ± SEM. Statistical significance was determined by two-way ANOVA followed by Student Newman–Keuls post hoc test. n = 3 biological repeats. TdTomato positive cells indicated AAV.

2/5-GfaABC1D-Cre targeted astrocytes. ***P < 0.001.

Figure 3. Selective astrocyte elimination in lumbar enlargement attenuated neuropathic pain. Change of weight (**A**), BMS scores (**B**), mechanical allodynia (**C-D**), cold hyperalgesia (**E**) and thermal hyperalgesia (**F**) in mice after astrocyte elimination. Sham group, n=30; sham+AAV group, n=30; SCI+AAV group, n=36; SCI+AAV+DT group, n=36. Arrow, 500 ng DT injection was performed on 31, 32 and 34 dpi (days post-injury). Left, left hindlimbs; right, right hindlimbs. i.p., intraperitoneal injection. Values are the mean ± SEM. Statistical significance was determined by two-way ANOVA followed by Student Newman–Keuls post hoc test. *P < 0.05, **P < 0.01, ***P < 0.001, SCI+AAV+DT group vs. SCI+AAV group.

Figure 4. Microglia in lumbar enlargement were activated after selective astrocyte elimination. (**A-B**), images of immunofluorescent staining using GFAP (green), Tuj1 (red) and IBA1 (white) as characteristic markers of astrocyte, neuron and microglia, respectively. n = 3 biological repeats. Scale bar, 200μm. (**C**), the histogram and statistical results of GFAP, IBA1 and Tuj1 fluorescence intensity in lesion area. (**D**), the heatmap showed that the transcripts of pro-inflammatory and anti-inflammatory microglial marker genes. n = 3 biological repeats. (**E-H**), the histogram and statistical results of IBA1 fluorescence intensity in lumbar enlargement. CU=cuneate fasciculus, GR=gracile fasciculus, LST=lateral spinothalamic tract, DLST=dorsolateral spinothalamic tract, VST=ventral spinothalamic tract, DSC=dorsal spinocerebellar tract, VSC=ventral spinocerebellar tract, SDH=superficial dorsal horn. Values are the mean ± SEM. Statistical significance was determined by two-way ANOVA followed by Student Newman–Keuls post hoc test. *P < 0.05, **P < 0.01, ***P < 0.001, SCI+AAV+DT group vs. SCI+AAV group.

Figure 5. Selective astrocyte elimination activated Type I IFNs signal. (**A**), the heatmap showed the DEGs between SCI+AAV+DT group and SCI+AAV group. (**B**), PPI networks analysis showed

the interaction of the DEGs between SCI+AAV+DT group and SCI+AAV group. (**C**), GO enrichment analysis revealed the dominant biological process of DEGs between SCI+AAV+DT group and SCI+AAV group. (**D**), KEGG pathway showed dysregulated signaling pathways between SCI+AAV+DT group and SCI+AAV group. (**E-F**), GSEA analysis showed the dysregulated signaling pathways between SCI+AAV+DT group and SCI+AAV group. (**G**), the heatmap showed that the critical genes expression involved in type I IFNs signal. n = 3 biological repeats.

Figure 6. The type I IFNs signal was activated in microglia after selective resident astrocyte elimination. (**A-B**), RT-PCR identified the effects of selective astrocyte elimination and DT injection alone on mRNA expression of type I IFNs signal genes. n = 3 biological repeats. *P < 0.05, **P < 0.01, ***P < 0.001. (**C-D**), images of immunofluorescent staining and statistical results using IRF7, ISG15 and STAT1 as critical proteins of type I IFNs signal and microglia marker IBA1. Scale bar, 200μm. n = 3 biological repeats. *P < 0.05, **P < 0.01, ***P < 0.001, SCI+AAV+DT group vs. SCI+AAV group. (**E**), images of immunofluorescent staining using IRF7, ISG15 and IBA1. Scale bar, 200μm. n = 3 biological repeats. (**F-G**), the mRNA expression of pro- and anti-inflammatory microglial markers and type I IFNs signal critical genes after 0.2 μg/mL LPS stimulation. n = 3 biological repeats. *P < 0.05, **P < 0.01, ***P < 0.001, Control group vs. LPS 0.2μg group. All values are the mean ± SEM. Statistical significance was determined by two-way ANOVA followed by Student Newman–Keuls post hoc test.

Figure 7. Interferon agonist (Ploy:IC) an STING agonist (ADU-S100 and DMXAA) significantly activated the type I IFNs signal in microglia. **A-F**, the mRNA expression levels of *Irf7, Irf7, Ifnb, Stat2, Isg15, Stat1*, and *Irf9* after stimulating with different concentrations of Ploy:IC, ADU-S100 and DMXAA. n = 3 biological repeats. *P < 0.05, **P < 0.01, ***P < 0.001, treatment group vs. control group. All values are the mean ± SEM. Statistical significance was determined by two-way ANOVA followed by Student Newman–Keuls post hoc test.

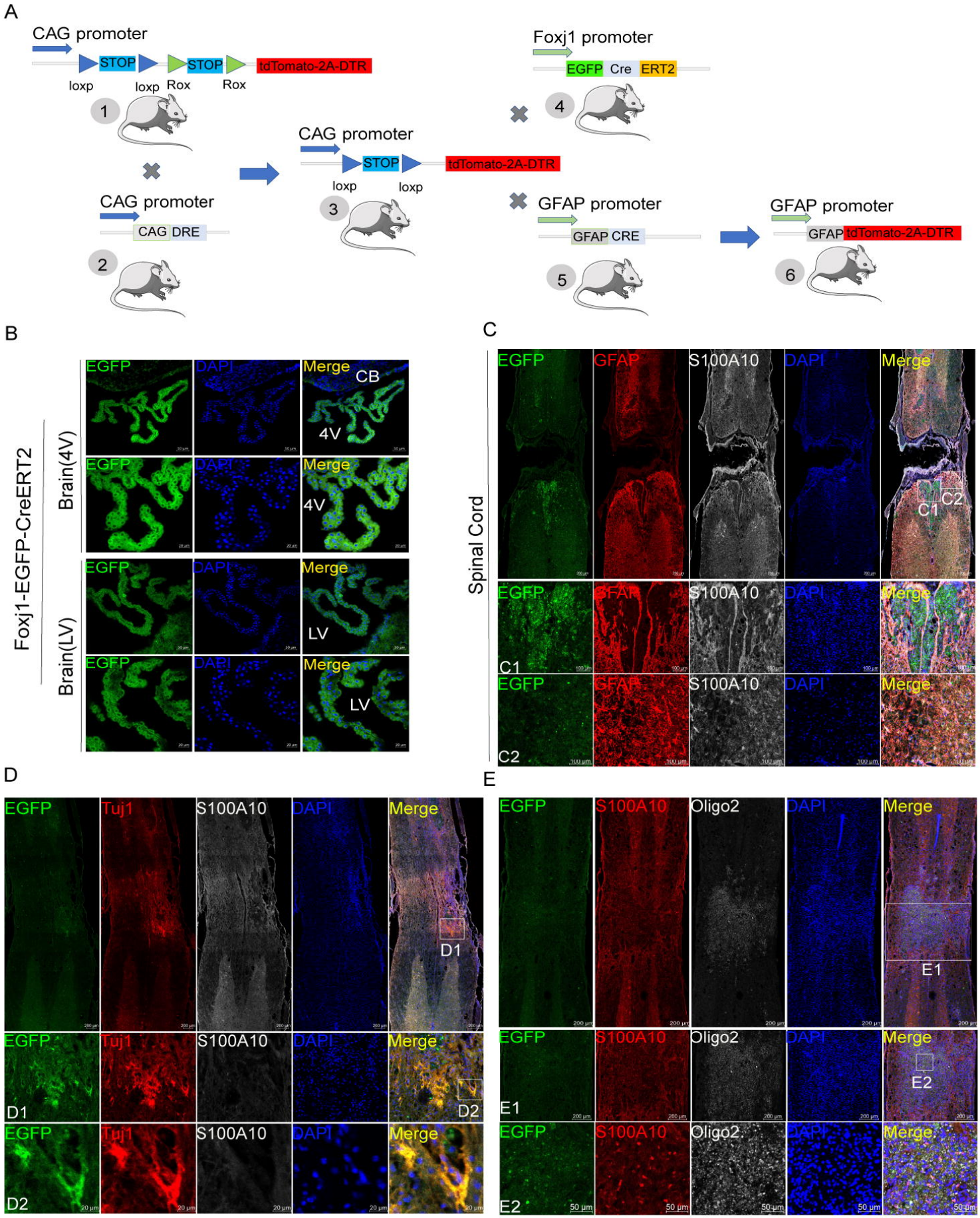
A
CAG promoter
STOP
STOP
tdTomato-2A-DTR
loxp
loxp
Rox
Rox
1
CAG promoter
CAG DRE
2
CAG promoter
STOP
tdTomato-2A-DTR
loxp
loxp
3
Foxj1 promoter
EGFP Cre ERT2
4
GFAP promoter
GFAP CRE
5
GFAP promoter
GFAP tdTomato-2A-DTR
6
B
Foxj1-EGFP-CreERT2
Brain(4V)
Brain(LV)
EGFP
DAPI
Merge
CB
4V
LV
C
Spinal Cord
EGFP
GFAP
S100A10
DAPI
Merge
C1
C2
D
EGFP
Tuj1
S100A10
DAPI
Merge
D1
D2
E
EGFP
S100A10
Oligo2
DAPI
Merge
E1
E2

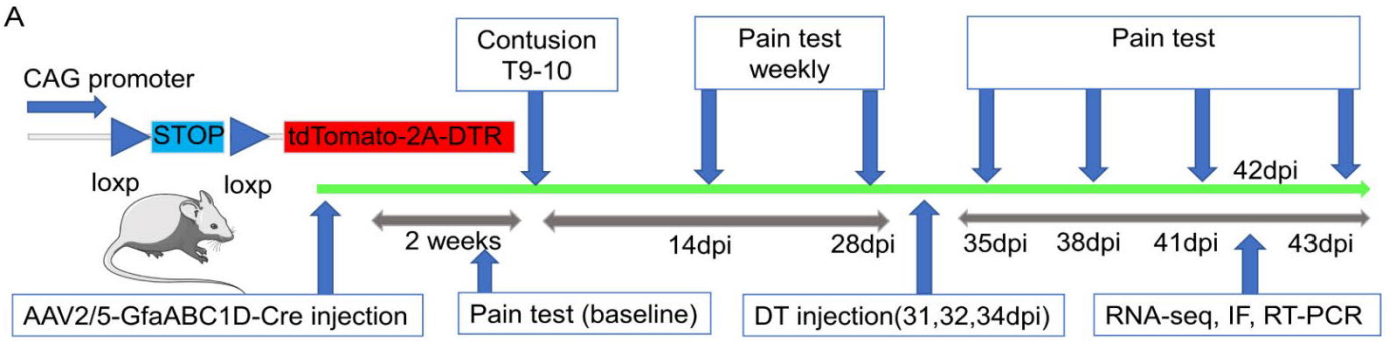
A
CAG promoter
STOP
tdTomato-2A-DTR
loxp
loxp
Contusion
T9-10
Pain test
weekly
Pain test
42dpi
2 weeks
14dpi
28dpi
35dpi
38dpi
41dpi
43dpi
AAV2/5-GfaABC1D-Cre injection
Pain test (baseline)
DT injection(31,32,34dpi)
RNA-seq, IF, RT-PCR

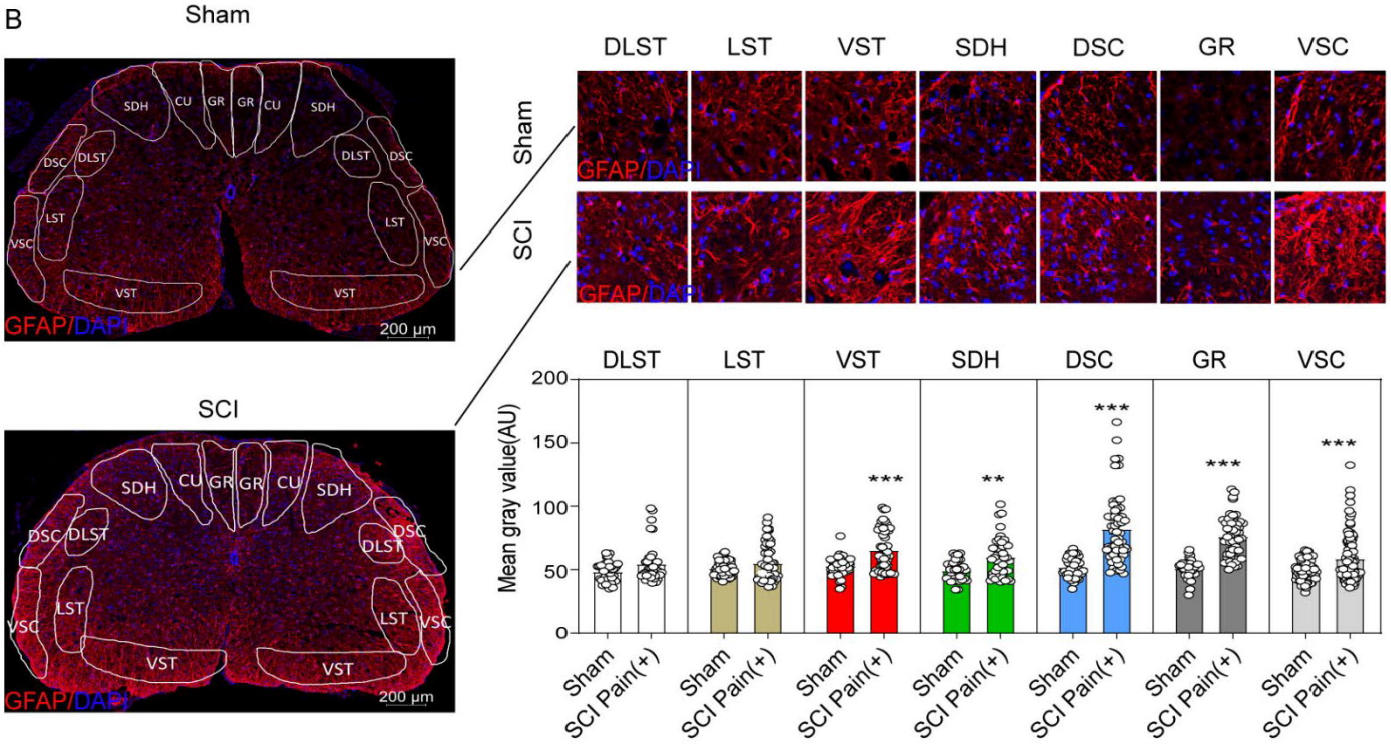
B
Sham
SCI
SDH
CU
GR
DSC
DLST
LST
VSC
VST
GFAP/DAPI
200 μm
DLST
LST
VST
SDH
DSC
GR
VSC
Mean gray value(AU)
Sham
SCI Pain(+)
***
**

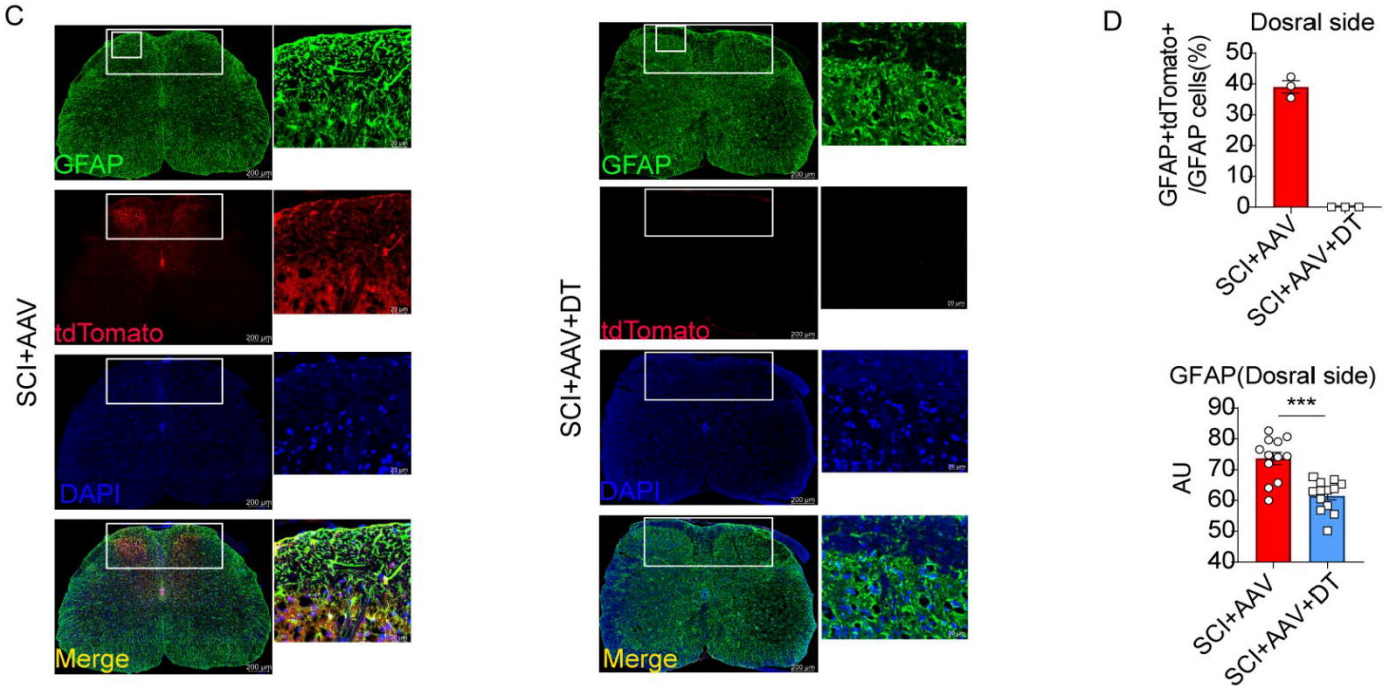
C
SCI+AAV
SCI+AAV+DT
GFAP
tdTomato
DAPI
Merge
D
Dosral side
GFAP+tdTomato+
/GFAP cells(%)
SCI+AAV
SCI+AAV+DT
GFAP(Dosral side)
AU
***

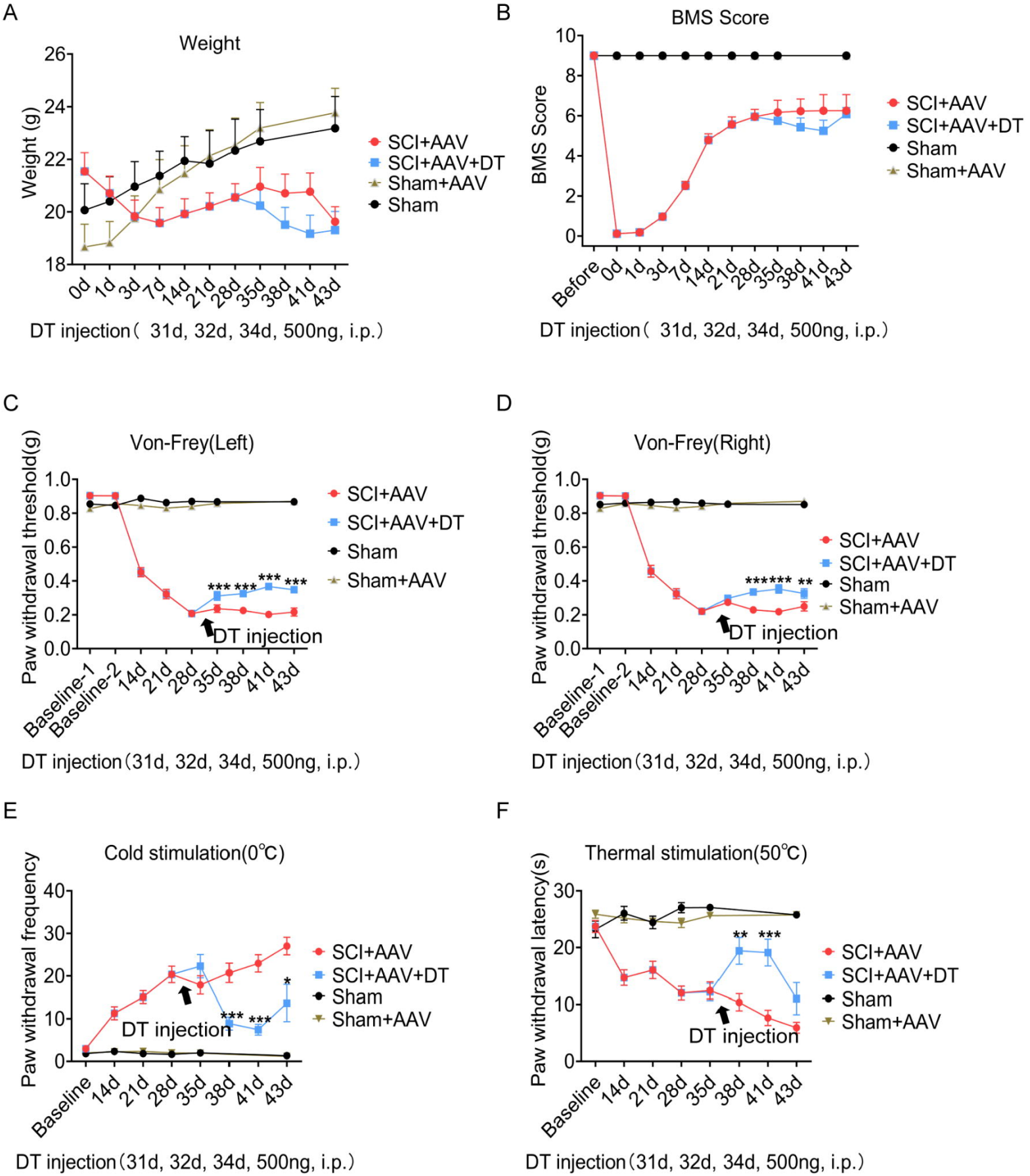
A
Weight
Weight (g)
26
24
22
20
18
0d 1d 3d 7d 14d 21d 28d 35d 38d 41d 43d
SCI+AAV
SCI+AAV+DT
Sham+AAV
Sham
DT injection（ 31d, 32d, 34d, 500ng, i.p.）
B
BMS Score
BMS Score
10
8
6
4
2
0
Before 0d 1d 3d 7d 14d 21d 28d 35d 38d 41d 43d
SCI+AAV
SCI+AAV+DT
Sham
Sham+AAV
DT injection（ 31d, 32d, 34d, 500ng, i.p.）
C
Von-Frey(Left)
Paw withdrawal threshold(g)
1.0
0.8
0.6
0.4
0.2
0.0
*** *** *** ***
DT injection
Baseline-1 Baseline-2 14d 21d 28d 35d 38d 41d 43d
SCI+AAV
SCI+AAV+DT
Sham
Sham+AAV
DT injection（31d, 32d, 34d, 500ng, i.p.）
D
Von-Frey(Right)
Paw withdrawal threshold(g)
1.0
0.8
0.6
0.4
0.2
0.0
****** **
DT injection
Baseline-1 Baseline-2 14d 21d 28d 35d 38d 41d 43d
SCI+AAV
SCI+AAV+DT
Sham
Sham+AAV
DT injection（31d, 32d, 34d, 500ng, i.p.）
E
Cold stimulation(0℃)
Paw withdrawal frequency
40
30
20
10
0
DT injection
*** *** *
Baseline 14d 21d 28d 35d 38d 41d 43d
SCI+AAV
SCI+AAV+DT
Sham
Sham+AAV
DT injection（31d, 32d, 34d, 500ng, i.p.）
F
Thermal stimulation(50℃)
Paw withdrawal latency(s)
30
20
10
0
** ***
DT injection
Baseline 14d 21d 28d 35d 38d 41d 43d
SCI+AAV
SCI+AAV+DT
Sham
Sham+AAV
DT injection（31d, 32d, 34d, 500ng, i.p.）

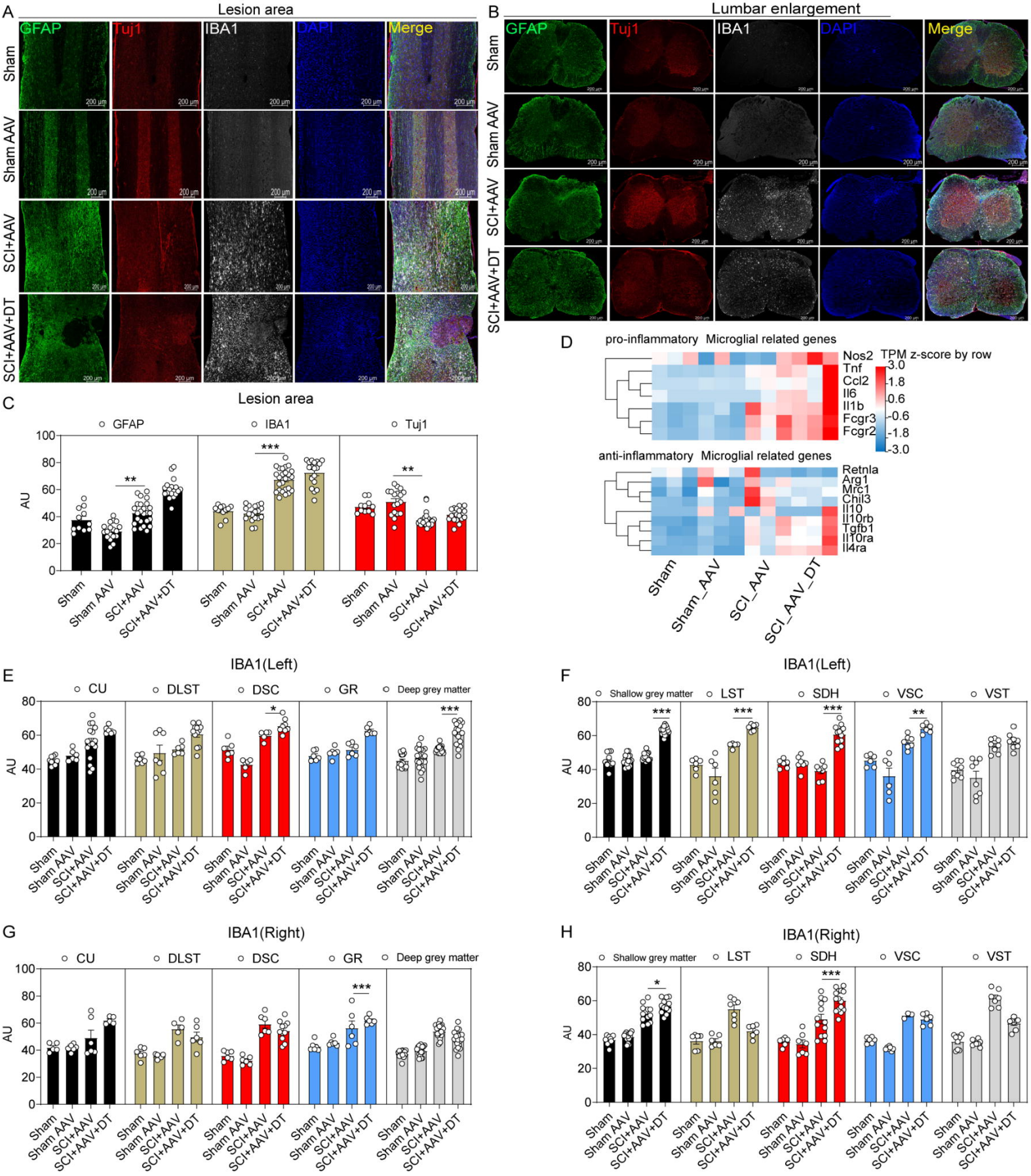
A
Lesion area
GFAP
Tuj1
IBA1
DAPI
Merge
Sham
Sham AAV
SCI+AAV
SCI+AAV+DT
200 μm
B
Lumbar enlargement
C
Lesion area
GFAP
IBA1
Tuj1
AU
Sham
Sham AAV
SCI+AAV
SCI+AAV+DT
D
pro-inflammatory Microglial related genes
Nos2
Tnf
Ccl2
Il6
Il1b
Fcgr3
Fcgr2
TPM z-score by row
anti-inflammatory Microglial related genes
Retnla
Arg1
Mrc1
Chil3
Il10
Il10rb
Tgfb1
Il10ra
Il4ra
Sham
Sham_AAV
SCI_AAV
SCI_AAV_DT
E
IBA1(Left)
CU
DLST
DSC
GR
Deep grey matter
F
IBA1(Left)
Shallow grey matter
LST
SDH
VSC
VST
G
IBA1(Right)
H
IBA1(Right)

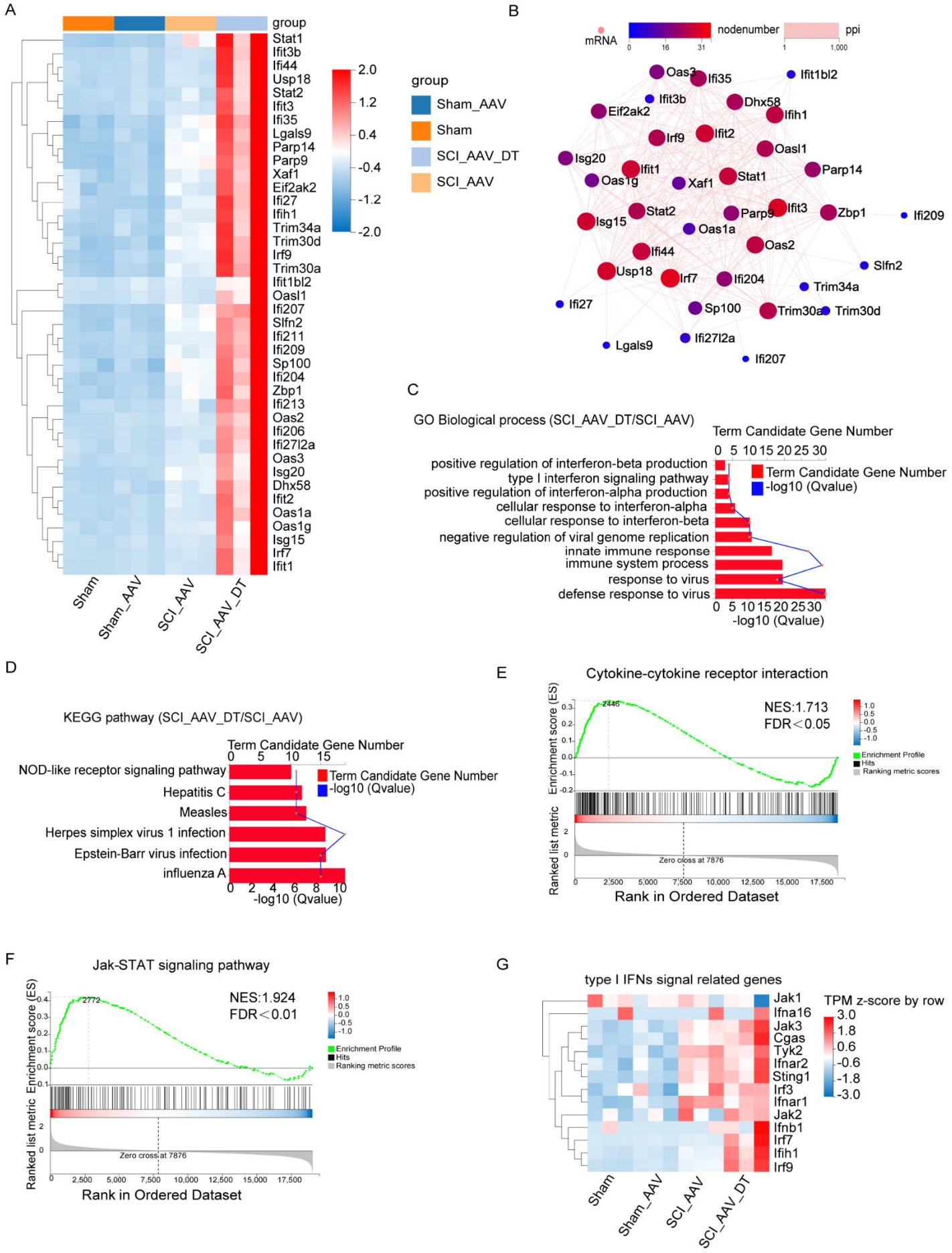
A
group
Stat1
Ifit3b
Ifi44
Usp18
Stat2
Ifit3
Ifi35
Lgals9
Parp14
Parp9
Xaf1
Eif2ak2
Ifi27
Ifih1
Trim34a
Trim30d
Irf9
Trim30a
Ifit1bl2
Oasl1
Ifi207
Slfn2
Ifi211
Ifi209
Sp100
Ifi204
Zbp1
Ifi213
Oas2
Ifi206
Ifi27l2a
Oas3
Isg20
Dhx58
Ifit2
Oas1a
Oas1g
Isg15
Irf7
Ifit1
Sham
Sham_AAV
SCI_AAV
SCI_AAV_DT
2.0
1.2
0.4
-0.4
-1.2
-2.0
group
Sham_AAV
Sham
SCI_AAV_DT
SCI_AAV
B
mRNA
nodenumber
ppi
C
GO Biological process (SCI_AAV_DT/SCI_AAV)
Term Candidate Gene Number
positive regulation of interferon-beta production
type I interferon signaling pathway
positive regulation of interferon-alpha production
cellular response to interferon-alpha
cellular response to interferon-beta
negative regulation of viral genome replication
innate immune response
immune system process
response to virus
defense response to virus
-log10 (Qvalue)
D
KEGG pathway (SCI_AAV_DT/SCI_AAV)
Term Candidate Gene Number
NOD-like receptor signaling pathway
Hepatitis C
Measles
Herpes simplex virus 1 infection
Epstein-Barr virus infection
influenza A
-log10 (Qvalue)
E
Cytokine-cytokine receptor interaction
NES:1.713
FDR<0.05
Enrichment score (ES)
Ranked list metric
Zero cross at 7876
Rank in Ordered Dataset
Enrichment Profile
Hits
Ranking metric scores
F
Jak-STAT signaling pathway
NES:1.924
FDR<0.01
Enrichment score (ES)
Ranked list metric
Zero cross at 7876
Rank in Ordered Dataset
G
type I IFNs signal related genes
TPM z-score by row
Jak1
Ifna16
Jak3
Cgas
Tyk2
Ifnar2
Sting1
Irf3
Ifnar1
Jak2
Ifnb1
Irf7
Ifih1
Irf9
Sham
Sham_AAV
SCI_AAV
SCI_AAV_DT

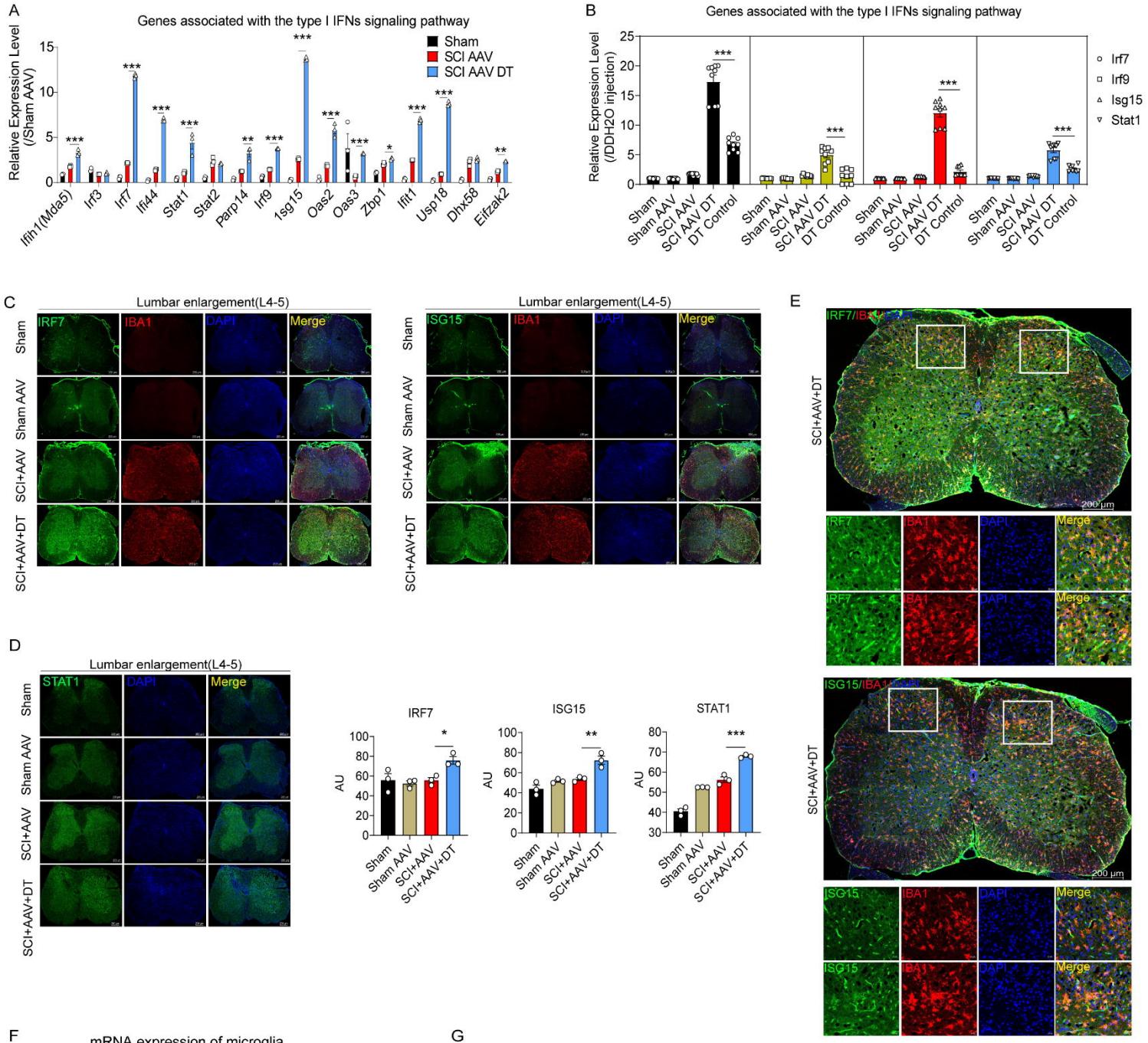
A
Genes associated with the type I IFNs signaling pathway
Relative Expression Level (/Sham AAV)
Sham
SCI AAV
SCI AAV DT
Ifih1(Mda5)
Irf3
Irf7
Ifi44
Stat1
Stat2
Parp14
Irf9
Isg15
Oas2
Oas3
Zbp1
Ifit1
Usp18
Dhx58
Eifzak2
B
Genes associated with the type I IFNs signaling pathway
Relative Expression Level (/DDH2O injection)
Irf7
Irf9
Isg15
Stat1
Sham
Sham AAV
SCI AAV
SCI AAV DT
DT Control
C
Lumbar enlargement(L4-5)
IRF7
IBA1
DAPI
Merge
ISG15
Sham
Sham AAV
SCI+AAV
SCI+AAV+DT
D
Lumbar enlargement(L4-5)
STAT1
DAPI
Merge
IRF7
ISG15
STAT1
AU
E
IRF7/IBA1/DAPI
ISG15/IBA1/DAPI
200 μm
F
mRNA expression of microglia
mRNA expression/GAPDH
Control
LPS 0.2μg
Tnfa
Il1b
Il6
Inos
Il4
Tgfb
Il10
Arg1
pro-inflammatory
anti-inflammatory
G
Genes associated with the type I IFNs signal
mRNA expression/GAPDH
Control
LPS 0.2μg
Sting1
Stat2
Stat1
Isg15
Irf9
Irf3

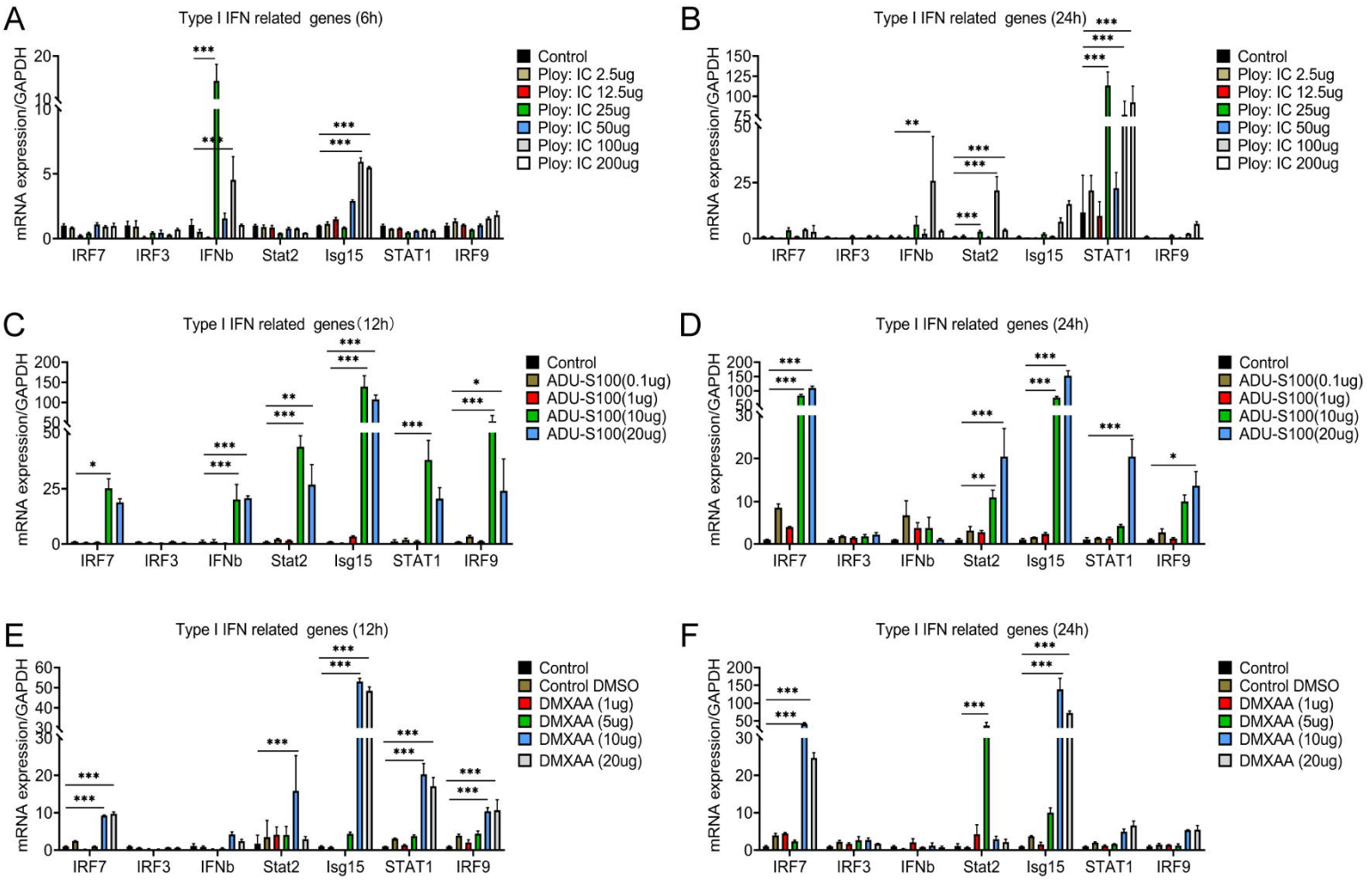
A
Type I IFN related genes (6h)
mRNA expression/GAPDH
IRF7
IRF3
IFNb
Stat2
Isg15
STAT1
IRF9
Control
Ploy: IC 2.5ug
Ploy: IC 12.5ug
Ploy: IC 25ug
Ploy: IC 50ug
Ploy: IC 100ug
Ploy: IC 200ug
B
Type I IFN related genes (24h)
C
Type I IFN related genes（12h）
ADU-S100(0.1ug)
ADU-S100(1ug)
ADU-S100(10ug)
ADU-S100(20ug)
D
Type I IFN related genes (24h)
E
Type I IFN related genes (12h)
Control DMSO
DMXAA (1ug)
DMXAA (5ug)
DMXAA (10ug)
DMXAA (20ug)
F
Type I IFN related genes (24h)